Alma Mater Studiorum · Università di Bologna

SCHOOL OF
ENGINEERING AND ARCHITECTURE
- Forlí Campus -

Master's Degree in Aerospace Engineering

Class LM-20

Graduation Thesis in:
Experimental methods in aerodynamics.

Setup and validation of a pulsed jet for turbulent boundary layer active control.

Candidate :
Lorenzo Magnani

Supervisor :
Prof. Gabriele Bellani

Session II
Academic Year 2022/2023

Abstract

The convective heat transfer enhancement is a very crucial topic. It possesses lots of industrial applications such as cooling of internal combustion engines or cooling of electronics, which in turn have an economical and environmental impact.
Most of the current experiments in this field aim at maximizing the heat exchanged by convection between a fluid and a wall, in a forced-convection regime. One solution is to employ active flow controls, in particular pulsed jets.
Pulsed jets acting on a cross flow generate distinct vortical structures, which interact with the wall. By changing several input parameters of the jet, it is possible to improve the heat transferred by convection.
Most of the control actions found up to now are validated at low Reynolds numbers. Therefore, it is important to find optimal solutions valid for high Reynolds number applications: the CICLoPE facility is the optimal structure for high Reynolds number experiments.
In particular, the objective of this thesis is to implement the jet that will be inserted in a high-Reynolds wind tunnel and to control the jet's input parameters such as pulsation frequency, duty cycle and output velocity.
A complete characterization of the jet has been performed, based on hot-wire anemometry, in order to have a full comprehension of the outcoming flow.

Key-words: Heat transfer, Convection, Flow control, Jet flow, Wall-bounded flows, Boundary layer.

Acknowledgements

"If you want to go fast, go alone; if you want to go far, go together".

This long degree journey is coming to an end: it took me many years, lots of difficult moments, bad news, hard times. I gave up many things, I missed many moments, I said no to many people; but I have no regrets. I did what it was necessary to realize my dreams, and I did it completely freely: I did what I wanted to do. But nothing of this would ever been even possible being alone. Many people have been close to me, and my biggest gratitude goes to you: I am where I am only because of you, even if you will never admit it.
First of all, I would like to thank my girlfriend: you're the strongest, kindest and most unpredictable person I will ever met. I would like to thank also my parents: you never had any doubts about me, even when I had. I'm so grateful to Rithvik, more a elder brother than a friend. I'm sincerely grateful to all my friends, both the ones from CICLoPE and the ones from my own city. And of course, a very big thanks goes to my professor Gabriele Bellani and my co-supervisor Lorenzo Larrazini.
Heartily, thank you all.

"Fairness, justice and freedom are more than words, they are perspectives".

Contents

List of Figures

List of Tables

.

Nomenclature

Abbreviations

A/D Analogue to Digital

AC Alternate Current

ADC Analogue to Digital Converter

BOS Background Oriented Schlieren

CCA Constant Current Anemometer

$CICLoPE$ Center for International Cooperation in LOng-Pipe Experiments

CTA Constant Temperature Anemometer

CVP Counter-rotating Vortex Pair

DAQ Data Acquisition system

DC Direct Current

DC Duty Cycle

div Divergence

$DTFT$ Discrete-Time Fourier Transform

FFT Fast Fourier Transform

$FPGA$ Field Programmable Gate Array

FS Full Scale flow

$grad$ Gradient

HDL Hardware Description Language

$JICF$ Jet In Cross Flow

LDA Laser Doppler Anemometry

PAT Planar Air Tunnel

PCB Printed Circuit Board

PDE Partial Differential Equation

PIV Particle Image Velocimetry

PLA PolyLactid Acid

PSD Power Spectral Density

$RANS$ Reynolds average Navier-Stokes equations

RTD Resistance Temperature Detector

$SLPM$ Standard Liter Per Minute

TBL Turbulent Boundary Layer

VDC Volt Direct Current

Symbols

$< U(x, y, z) >$ Mean value of a random variable

α Thermal diffusivity of the fluid

α_r Electrical resistivity

α_t Overheat ratio

β Coefficient of volume expansion

ΔU Variation of the internal energy

δ_{ik} Kronecker delta

ϵ Energy dissipation rate

η Kolmogorov's length scale

$\frac{\partial}{\partial t}$ Partial derivative

$\frac{D}{Dt}$ Total derivative

γ Ratio between specific heat at constant pressure and specific heat at constant volume

λ Therma conductivity of the material

μ Dynamic viscosity

ν Kinematic viscosity

Φ Dissipation function

ρ Density

τ Viscous stress tensor

τ_{wall} Wall shear stress

$\underline{U}\,(x, y, z, t)$ Instantaneous value of a random variable

Bi Biot number

C_f Skin friction coefficient

C_p	Specific heat at constant pressure
d, D	Representative dimension of the problem
e	Internal energy per unit mass
F	Resultant of the volume forces
f	Body forces per unit mass
g	Gravitational acceleration
Gr	Grashof number
h	Convective heat transfer coefficient
K	von Kármán constant
k	Thermal conductivity of the fluid
l_*	Length scale in inner units
M	Mach number
Nu	Nusselt number
p	Pressure
p_0	Total pressure
p_1	Static pressure
Pr	Prandtl number
Q	Heat introduced in unit time inside the considered volume of fluid
q	Heat flux vector
q_c	Convective heat flux

q_j Heat flux by Joule effect

q_r Radiative heat flux

q_{tan} Conductive heat flux

Re Reynolds number

Re_τ Friction Reynolds number

S Entropy of the system

St Stanton number

T Temperature

t Time

T_∞ Bulk temperature

T_s Temperature of the surface

$u\,(x, y, z, t)$ Fluctuating value of a random variable

U^+ Inner-scaled velocity

u_τ Friction velocity

V Velocity

V Voltage value

V_{corr} Voltage after temperature correction

V_{ds} Drain-to-source Voltage

V_{gs} Gate-to-source Voltage

W_τ Work done in unit time by the surface forces connected with the deviatoric part of the stress tensor

W_f Work done in unit time by the body forces

W_p Work done in unit time by the surface forces connected with the isotropic part of the stress tensor

y^+ Distance from the wall in inner units

Chapter 1

Introduction

The objective of my thesis work is the enhancement of the heat exchange by convection between a fluid and a wall, because it is a relevant phenomenon in many industrial applications.
Nowadays, controlling the heat exchange is particularly important especially in all those applications in which temperature control becomes relevant. As a matter of fact, temperature is a limiting factor in lots of industrial applications, such as internal combustion engines or electronic circuits. For instance, one of the main factors inhibiting the development of faster microchips that exist today is the effective removal of the heat generated within the chips. [1]
Furthermore, the thermal efficiency of most combustion engines is rarely higher than 55%. This means that actual engines can convert into useful work only half of the heat that is generated by combustion: the remaining part is lost, in the sense that does not create useful work.
One of the reasons behind these low thermal efficiencies is that the materials employed in the warmer parts cannot withstand all the heat generated by the combustion process. Therefore, by increasing the maximum operating temperature of the warmer parts (combustion chamber, turbine blades) it is possible to increase the thermal efficiency.
Controlling the heat exchange is also exploited for preventing the rise of thermal gradients which can alter, for example, the reliability of ultrasonic inspection tech-

niques. This happens because the speed of sound depends on the temperature inside the travelling medium, therefore temperature variations cause an acoustic signal's distortion. [2]

Another relevant aspect concerns the rise in energy consumption due to the significant growth in the population in many countries. Since fossil fuels are costly and pollute the environment, governments promote ideas on using optimized and energy-efficient equipment. A very interesting research done by Zhang et al. [3], investigated the relationship between the two variables of energy consumption and economic growth. The results show that energy consumption and economic growth have a long-term relationship with each other and a bilateral causality relationship is established between them. These are only few examples explaining why thermal management has become an attractive research topic.

Aerodynamicists are very good candidates to study heat, because it is strongly connected with turbulence. As a matter of fact, it is well known that the heat transfer between a solid and a fluid is significantly different between a laminar or a turbulent flow.

Turbulence is a physical phenomenon concerning fluids (liquids and gases), but even though the constitutive equations describing their dynamic are known since 1822, their comprehension is still not complete.

As a matter of fact, Navier-Stokes equations are so complex even without the use of the latest physical theories (general relativity, quantum mechanics) that their solution is one of the so called "Millennium problems".

The concept of turbulence is very important, because in most of the industrial applications, flows are in a turbulent regime: they are usually referred to as "wall-bounded" or "near-wall" turbulent flows. Actually there is lots of literature explaining the theory behind heat exchange mechanisms, and the technological progress allows to perform very thorough experiments. A particular remark deserves the work of Castellanos et al[4], in which a parametric study about an impinging jet in cross-flow is carried out in order to find specific control actions to increase the heat exchanged by convection.

But most of recent experiments in the field of heat transfer enhancement are limited

to low Reynolds number, while the nature and most of the industrial implementations operate at much higher Reynolds number.
This is the driving factor of my thesis work: the validation of the heat transfer enhancement by convection throughout the use of an active flow control, at high Reynolds numbers. This task is accomplished by developing an impinging jet in cross-flow controlled in frequency, duty cycle and velocity, and assessing its effectiveness inside a high Reynolds number facility, i.e. the CICLoPE wind tunnel.

1.1 Thesis objective

The thesis objectives can be summarized as follows:

- Literature review of the articles concerning the heat transfer enhancement with active methods;
- Implementation of a setup that generates a pulsed jet controlled in frequency, duty cycle and output velocity;
- Characterization of the outcoming flow and validation of the input parameters.

This thesis can be summarized by the following questions:

1. What are the main parameters that influence the heat transferred by convection?
2. Is my setup able to generate a pulsed jet and to control those parameters?
3. Which are the following steps of this thesis?

Answers will be given in the following chapters.

1.2 Thesis outline

The structure of this elaborate is the following:

- Chapter 2 provides the mathematical and theoretical explanation of all the topics that will be treated in this dissertation. It starts with the governing equations of the motion of fluids; then it treats the laws that regulate the transfer of the heat between two bodies. Successively a brief explanation of turbulence features is carried out, with a focus about wall-bounded flows and jet flow. Finally, a study about the state of the art about the heat transfer enhancement techniques is conducted;

- Chapter 3 describes important experimental procedures at the basis of the experimental results that I have obtained. In fact, all the experimental techniques here treated derive their working principle in the equations shown in Chapter 2. The equations also explain why the CICLoPE laboratory is a unique structure in the world, and an optimum candidate for this research topic;

- Chapter 4 treats in detail all the experimental instruments employed during the thesis, and what are the working principles behind a data-acquisition procedure;

- Chapter 5 presents all the experimental results that have been collected in order to have an as complete as possible characterization of the output flow;

- Chapter 6 gives an answer to the question at the basis of this work. Additionally, some tips for future works or improvements are suggested.

Chapter 2

Theoretical background

Fluid dynamics is the science that describes the motion of fluids and studies its effects on surrounding or immersed bodies.
It is always incredible to see how many applications this "simple" definition possesses, most of which can be appreciated in everyday life. Indeed, fluid dynamics allows to explain the motion of blood in the human body, but also to make weather predictions; it can be used to study the flight of different animals(birds, insects), but also the performance of every vehicle that moves inside the atmosphere.
In the discussion of the constitutive equations proposed in the next section, turbulence is treated as a flow characteristic.

2.1 Navier-Stokes equations

Mathematics is the most efficient language ever by which the human being has been able to describe the nature. Therefore, as every scientific subject, the description of the motion of fluids is possible by means of appropriate mathematical models, which rely on several assumptions.
These approximations, posed in order to simplify the mathematical description of what we can observe, are very important because underline the limits of applicability of the model.

The fundamental equations are:

$$\frac{\partial \rho}{\partial t} + V \cdot grad\, \rho + \rho div\, V = 0; \tag{2.1}$$

$$\rho \left(\frac{\partial V}{\partial t} + V \cdot grad\, V \right) = \rho f - grad\, p + div\, \tau; \tag{2.2}$$

$$\rho \left(\frac{\partial e}{\partial t} + V \cdot grad\, e \right) = -p\, div\, V + \Phi - div\, q. \tag{2.3}$$

The constitutive equations are:

$$p = p\left(\rho, T\right); \tag{2.4}$$

$$e = e\left(\rho, T\right); \tag{2.5}$$

$$q = -k\, grad\, T; \tag{2.6}$$

$$\tau_{ik} = -\frac{2}{3}\mu div\, V\, \delta_{ik} + \mu \left(\frac{\partial u_i}{\partial x_k} + \frac{\partial u_k}{\partial x_i} \right); \tag{2.7}$$

$$\Phi = \tau : grad\, V. \tag{2.8}$$

This set of equations provides the mathematical description of the motion of a Newtonian fluid. Only after introducing the constitutive equations, Equations (2.1, 2.2, 2.3) form a system of 5 equations in 5 unknowns. But this it is not sufficient in order to make predictions for generic flow problems: as a matter of fact, the fundamental equations form a set of coupled and Partial Differential Equations (PDE).

The fact that they are coupled implies that all the unknowns are obtained by solving the whole set of equations *simultaneously*.

But the most complicating property is the non-linearity, which prevents from the use of many mathematical and numerical procedures that exploit this property. Indeed it is well known that even a little change in the initial conditions, produces a completely different result.

2.1.1 Continuity equation

Equation 2.1 is derived by applying the localization lemma to the differential form of the equation for the *balance of mass*, reported in equation 2.9:

$$\frac{D}{Dt}\int_{v(t)} \rho \, dv = 0. \tag{2.9}$$

This equation states that the mass of a material volume of fluid does not change in time, which is equivalent to say that inside a material volume, no creation or destruction of mass may occur.[5]

2.1.2 Momentum equation

Equation 2.2 is the so called "momentum balance equation", whose original mathematical expression is 2.10:

$$\frac{D}{Dt}\int_{v(t)} \rho \, V \, dv = F. \tag{2.10}$$

The momentum balance asserts that the variation in unit time of the momentum of a material volume of fluid is equal to the resultant of the forces acting on the volume itself. [5]

2.1.3 Balance of total energy

Equation 2.3 represents a *balance of total energy*, which is the sum of the internal and kinetic energy of the material volume taken into account. The mathematical expression is 2.11:

$$\frac{D}{Dt}\int_{v(t)} \rho\left(e+\frac{V^2}{2}\right) dv = W_f + W_p + W_\tau + Q. \tag{2.11}$$

where on the right hand side appear different forms of work performed and the heat introduced in unit time.

This equation reads as follows: the variation in unit time of the total energy of a material volume of fluid is equal to the sum of the work done in unit time by the forces acting on the volume and of the heat introduced in unit time through its bounding surface.[5]

2.2 Thermodynamic equations

Thermodynamic is the science that studies the relationships between heat, work, temperature, and energy. In particular, the laws of thermodynamics describe the variations in the energy state of a system and its ability to perform useful work on its surroundings.

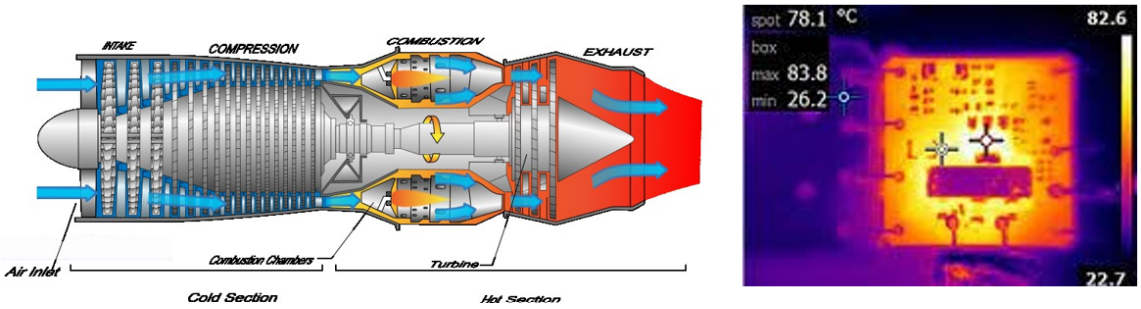

Figure 2.1: Applications for the heat transfer enhancement: on the left, a jet engine[6]; on the right, a motherboard circuit[7].

The key concept is that heat is a form of energy corresponding to a definite amount of mechanical work.[8]

It is important to make a clear distinction between two quantities: temperature and heat. Based on the kinetic theory of gases, the *heat* is a form of energy connected with the kinetic energy of the molecules; the *temperature* is a macroscopic measure of

this energy level. In general, if the temperature between two bodies is not uniform, then transport of heat will occur. [9]

2.2.1 Fundamental laws of thermodynamics

The fundamental laws of thermodynamics are briefly discussed. Many famous physicists and engineers contributed to their drafting: Sir Benjamin Thompson, Sadi Carnot and Rudolf Clausius are only some of the most renowned names.
These equations are the mathematical laws,based on a fundamental set of postulates, that govern the exchange of heat between different bodies.

1. *The zeroth law of thermodynamics* states that when two systems are each in thermal equilibrium with a third system, the first two systems are in thermal equilibrium with each other. This property makes it meaningful to use thermometers as the "third system" and to define a temperature scale.

2. *The first law of thermodynamics* affirms that the variation in a system's internal energy is equal to the difference between the work done by the system on its surroundings and the heat added to the system from its surroundings. In other words, energy cannot be created or destroyed, but merely converted from one form to another(even thought there is no limit in this conversion). This law is also known as "law of conservation of energy" and its general equation is 2.12:

$$\Delta U = \Delta Q + \Delta W, \tag{2.12}$$

   where U is the internal energy function, Q is the heat and W is the work.

3. *The second law of thermodynamics* asserts that heat does not flow spontaneously from a colder region to a hotter region, or, equivalently, heat at a given temperature cannot be converted entirely into work. Consequently, the entropy of a closed system, increases over time toward some maximum value. Thus, all closed systems tend toward an equilibrium state in which entropy is at a maximum and no energy is available to do useful work. It is important to

recall that the entropy is defined as:

$$S(A) = \int_0^A \frac{dq}{T} \Rightarrow dS = \frac{dQ}{T}. \tag{2.13}$$

where a reversible transformation moves the system from state "0" (fixed state) to the general equilibrium state "A".

2.2.2 Heat transfer

Heat is exchanged through 3 main mechanisms: conduction, radiation and convection.
The heat transferred by convection occurs due to the bulk movement of molecules within the liquid, gas, or liquid-gas mixture, and this thesis focuses on this particular mechanism. Initially, heat is transferred between molecules via conduction, but the main heat transfer is via the motion of molecules within the fluid.
This convective movement can take two forms:

- *Natural convection*: this phenomenon is caused by buoyant forces due to a difference in density connected to temperature differentials. When the fluid comes in contact with a hot surface or atmosphere, the molecules are separated and scattered, reducing the fluid's density;

- *Forced convection*: it occurs when the fluid undergoes forced flow from an outside source such as a water heater, pump, or fan.

When dealing with convection processes, it is common to use the Nusselt number (Nu), that is the dimensionless parameter characterizing convective heat transfer. It expresses the ratio between the flow of heat exchanged by convection and the flow of heat exchanged by conduction.
The Nusselt number definition comes by making the differential form of the Fourier's law of thermal conduction non-dimensional, and can be expressed through the following relationship:

$$Nu = \frac{h \cdot d}{k}. \tag{2.14}$$

where:

- h is the convective heat transfer coefficient;
- d is the representative dimension, which depends on the particular case (e.g., diameter for pipes);
- k is the thermal conductivity of the fluid.

The unitary Nusselt value is characteristic of heat transferred by pure conduction through the fluid layer; as the value of Nu increases, the phenomenon of convection becomes more and more developed.
Generally the Nusselt number is evaluated as a function of the Prandtl number and, if the convection is natural, of the Grashof number. If instead it is forced, it is a function of the Reynolds number, up to a coefficient C and of the exponents n and m to which they are elevated the other two dimensionless groups. In particular, in the case of natural convection it can be expressed by the following relationship:

$$Nu = C \cdot Gr^n \cdot Pr^m. \tag{2.15}$$

while in the case of forced convection it can be determined by the following equation:

$$Nu = C \cdot Re^n \cdot Pr^m. \tag{2.16}$$

The Prandtl number (Pr) is a dimensionless number defined as the ratio of momentum diffusivity to thermal diffusivity. The Prandtl number is given as:

$$Pr = \frac{\nu}{\alpha} = \frac{C_p \mu}{k}; \tag{2.17}$$

where α is the thermal diffusivity, μ is the dynamic viscosity, k is the thermal conductivity and C_p is the specific heat at constant temperature.

On the other hand, the Grashof number (Gr) is a dimensionless number which approximates the ratio of the buoyancy to viscous forces acting on a fluid.

$$Gr = \frac{g \cdot \beta \left(T_s - T_\infty\right) D^3}{\nu^2}; \tag{2.18}$$

where g is the gravitational acceleration, β is the coefficient of volume expansion, T_s is the surface temperature, T_∞ is the bulk temperature and D is the characteristic pipe length.

2.3 Turbulent scales

Even if turbulence is a common phenomenon of our daily lives, there is not a coherent definition; indeed, turbulence is a phenomenon that presents some specific characteristics:

- It is a "disorder" motion: the term "randomic" is avoided on purpose, because even if the motion cannot be reproduced in details, different interacting scales can be recognized;
- It presents enhanced mixing, heat and mass transfer: indeed, turbulent mixing is more effective than molecular mixing;
- It presents high level of 3-D fluctuations;
- It is a high Reynolds number phenomenon.

The latter feature is important, because it is indicative of a large scale separation, both time and spatial scales, which interact during the motion.
The largest scales are the one associated with the macroscopic geometry of the body in which the flow is developing: for a pipe flow is the radius of the pipe. The smallest scales are the ones in which viscosity acts, and dissipates the energy generated at the largest scales.

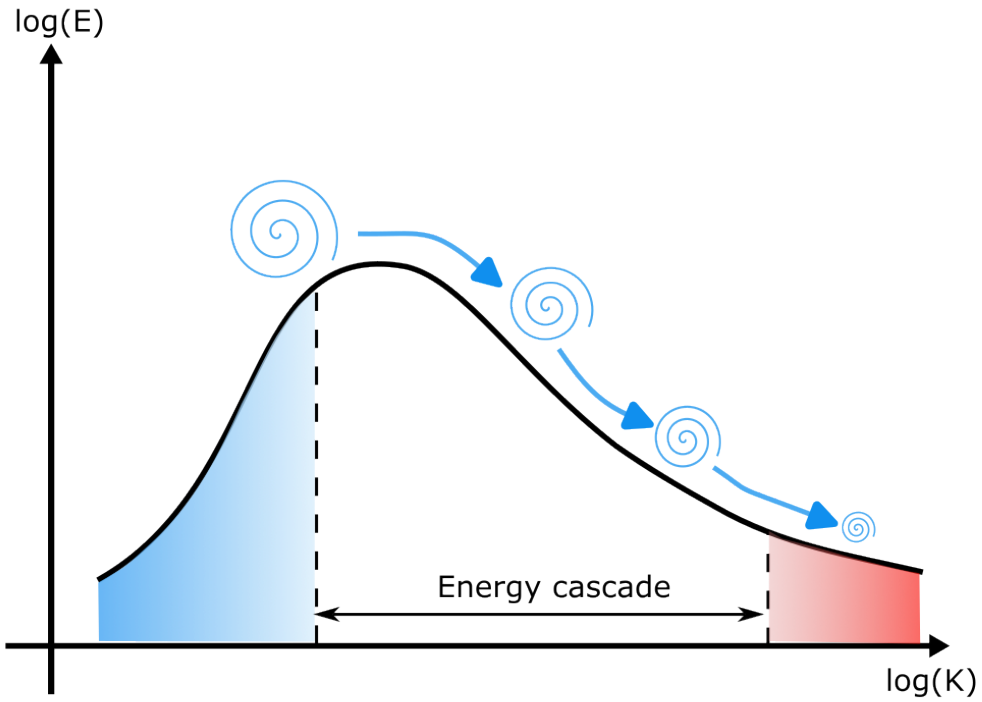

Figure 2.2: Energy cascade process.[10]

The energy of the turbulent motion comes from the biggest scales, which get their energy from the mean flow throughout a production mechanism. Then, the energy is transferred to smaller and smaller scales via an inviscid process. This goes on up to a point in which the size of the eddies becomes so small that are dissipated by viscosity.

According to Richardson, the scales are characterized by a length scale, a time scale and a velocity scale. For the large scales, the length scale is dictated by the flow geometry (R) and the velocity scales can be associated to the mean velocity of the flow(U).

But as the cascade process continues, this large eddies break up, and their dimensions reduce up to a value in which the local Reynolds number becomes almost equal to 1. Hence, Re = 1 is the limit that sets the size of the smallest scales (η) : after

this point, viscosity can act, and the energy is dissipated into heat. Therefore, the smallest scales can be assumed to be isotropic, because any macroscopic information got lost in the cascade process. Or, in other words, the smallest scales are "*universal*".

This is one of the hypotheses at the basis of the Kolmogorov's theory, that aimed at determining the length scale of the smallest scales. The second assumption states that, if the Reynolds number is sufficiently high, the statistics of the small scales are universal and determined by only two parameters: ν and ε. ν is the kinematic viscosity, ε is the energy dissipation rate. The definition of the Kolmogorov's length scale can be derived from the second assumption and via a dimensional analysis:

$$\eta = \nu^a \cdot \epsilon^b \Rightarrow \eta = \left(\frac{\nu^3}{\eta}\right)^{\frac{1}{4}} \tag{2.19}$$

By writing the ratio between the largest and the smallest scales, and assuming that $\varepsilon$is equal to the energy input (U^3/R), one gets:

$$\frac{R}{\eta} = Re^{\frac{3}{4}} \tag{2.20}$$

This is the formula that describes the scale separation phenomenon, that is by increasing the Re the range of available scales increases; this happens because the smallest scales become smaller and smaller.

2.4 Wall-bounded(turbulent) flows

Since one of the goals of this thesis would have been the validation of the experimental setup inside the CICLoPE wind tunnel, the main characteristics of such a flow must be taken into account.
Wall-bounded flows are flows characterized by the fact that at least one side of the fluid is in contact with a wall: boundary layer flow, channel flows and pipe flows belong to this category. Since in most of everyday applications the flow is in a turbulent regime, the description focuses on turbulent wall-bounded flows.

For the description of these kind of flows, the Navier-Stokes equations are not the most suitable model. As a matter of fact, even with the approximation of incompressible flow and neglecting the body forces, these equations are not used because provide an instantaneous description of the flow. Since the development of a turbulent flow is not deterministic, this kind of description reveals not to be the most appropriate.
Therefore the description of the mean flow field is preferred, and the equations that make it possible are the so called "Reynolds-Averaged Navier-Stokes" equations (**RANS**). As the name suggests, they are obtained by applying the Reynolds decomposition to all the fluctuating quantities inside the Navier-Stokes equations. [11] In this case, statistically-stationary and fully-developed flow is considered.

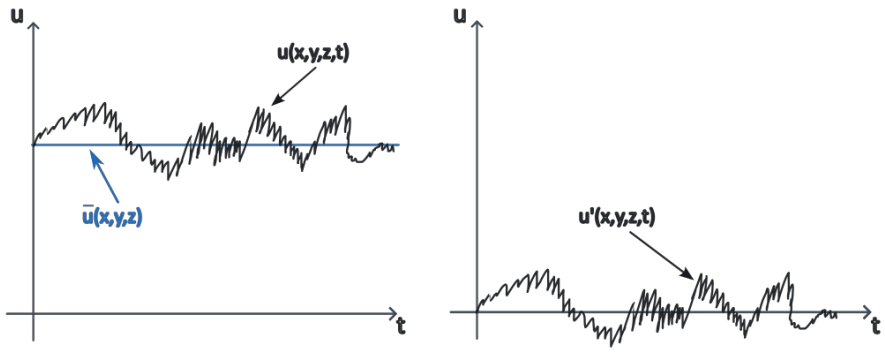

Figure 2.3: Reynolds decomposition of a random signal.

The Reynolds decomposition separates each random variable into its mean value plus its fluctuating component:

$$\underline{U}\,(x,y,z,t) =< U\,(x,y,z) > +u\,(x,y,z,t)\,. \tag{2.21}$$

Since the flow is turbulent, the fluctuating/random variables are the velocity and the pressure; therefore, by applying 2.21 to these quantities according to some averaging rules, the RANS can be written as follows:

$$\frac{\partial u_i}{\partial x_i} = 0. \tag{2.22}$$

$$\frac{D < U_i >}{Dt} = -\frac{1}{\rho}\frac{\partial < P >}{\partial x_i} + \frac{1}{\rho}\frac{\partial}{\partial x_j}\left[< \tau_{ij} > -\rho < \mathbf{u_i u_j} >\right]. \tag{2.23}$$

Finally, by assuming 2-D flows and that changes in the x direction happen much slower than changes in the y direction and performing an order of magnitude estimation, the Thin-Shear Layer equation is derived.

$$U\frac{\partial U}{\partial x} + V\frac{\partial U}{\partial y} = -\frac{1}{\rho}\frac{dP_0}{dx} + \frac{\partial}{\partial y}\left[\nu\frac{\partial U}{\partial y} - < uv >\right]. \tag{2.24}$$

This equation comes from the x momentum equation, and the first term inside the square brackets is called the "viscous term".

2.4.1 Wall-bounded turbulent scaling

In general, equation 2.24 describes the behaviour of flows inside a thin region of concentrated vorticity across which the tangential velocity component varies greatly. Therefore, it can be used in order either to describe:

- jets, wakes, mixing layer flows. These are known as *free-shear layer flows*, for which the viscous term can be neglected;
- pipe flows, channel flow, boundary layer flow. They are called *wall-bounded flows*, and the viscous term cannot be neglected, because is a term directly linked to the no-slip boundary condition.

Prandtl divided the turbulent boundary layer mean velocity profile into an **inner region**, close to the wall, and an **outer region**, far from the wall. These two regions are considered to be separated, based on the assumption that the inner region is influenced by viscous forces, while in the outer region the inertial forces are dominant.

Therefore, one velocity scale and one length scale for each region are needed, for a

correct self-similar description of wall-bounded flows.
For the outer region, the velocity at the center-line U_0 and the characteristic dimension of the geometry δ can be used. Inside this region any information about the viscosity is lost, and the scaling law is the so called **"defect law"**, proposed by von Kármán.
For the inner region, the "law of the wall" scaling law applies (introduced by Prandtl) and the flow has lost any information about the larger scales. Here, the friction velocity is introduced:

$$u_\tau = \sqrt{\frac{\tau_w}{\rho}}. \tag{2.25}$$

where τ_w is the wall shear stress. Once defined the friction velocity, the viscous length scale l_* and the inner-scaled velocity U^+ are derived as follows:

$$l_* = \frac{\nu}{u_\tau}. \quad U^+ = \frac{U}{u_\tau}. \tag{2.26}$$

Therefore by applying 2.26 to the momentum equation for turbulent wall-bounded flow, the inner-scaled momentum equation is obtained:

$$1 - \frac{y^+}{h^+} = \frac{\partial U^+}{\partial y^+} - < uv >^+ . \tag{2.27}$$

where the "+" symbol refers to inner-scaled variables, i.e. variables divided or by u_τ or by l_*.
Equation 2.27 allows to divide wall-bounded flows into several areas in which some terms of Equation 2.27 can be neglected:

- Viscous sublayer →Here the effects of viscosity are dominant over all the other effects; it extends from the wall up to $y^+<5$;
- Buffer layer →Here the Reynolds shear stress term is of the same order of viscous term; it extends from $5 \leq y^+ \geq 100$;
- Overlap layer →Here the effects of the Reynolds shear stress term are dominant over all the other effects; it goes from $100 \leq y^+ \geq 0.15\ \delta$;

- Core region →It goes from y^+ >0.15 δ up to the center line, and completely belongs to the outer region.

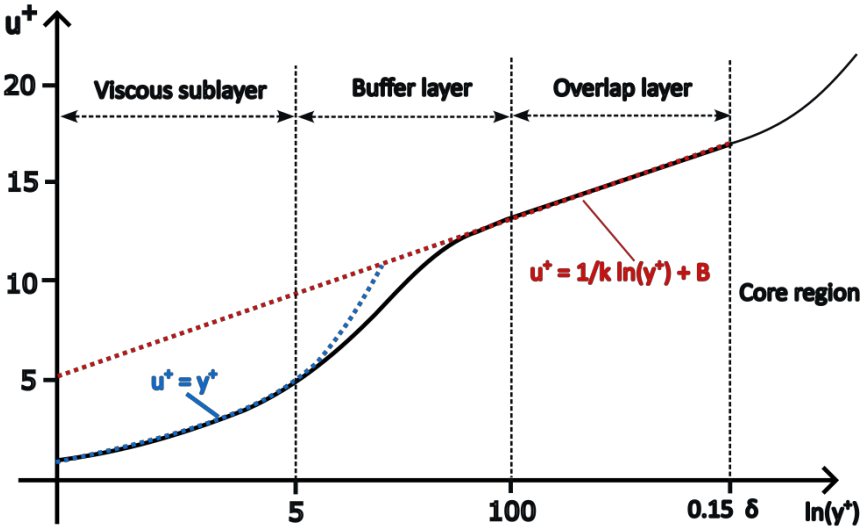

Figure 2.4: Logarithmic law[12].

The two scaling laws, i.e. the law of the wall and the defect law overlap in the *overlap layer* : the combination of these two scaling laws culminates in the **logarithmic law**, or simply "log law".

$$U^+ = \frac{1}{K}\, ln\, y^+ + C. \tag{2.28}$$

In this equation, K is the von Kármán constant, whose value is of extreme importance for the modelling of wall-bounded flows; CICLoPE wind tunnel has been developed for the very reason of extracting its value more easily.

2.5 The Reynolds analogy

The Reynolds analogy is an approach to forced convection based on similarities between the equations for heat transfer and momentum transfer. In other words, the

geometric similarity of the momentum boundary layer and the thermal boundary layer is used to express a relationship between the shear force at the wall (due to viscous drag) and the total heat transfer at the wall (due to thermal diffusivity). This provides a useful way to estimate heat transfer rates in situations in which the skin friction is known.
As a matter of fact, in a turbulent flow the velocity and the temperature profiles have the same shape. This happens because the transport of momentum and the transport of heat largely depend on the same turbulent eddies, rather than on natural diffusion process. Therefore the following relationship is valid:

$$St = \frac{f}{2}; \tag{2.29}$$

where $f = \dfrac{2\tau}{\rho u^2}$ is the Fanning friction factor, and St is the number used to characterize heat transfer in forced convection flows[13]. It expresses the ratio of heat transferred into a fluid to the thermal capacity of fluid:

$$St = \frac{Nu}{Re \cdot Pr}; \tag{2.30}$$

This analogy is no longer valid in all those situations in which the previous assumptions are not satisfied. As an example, when liquids, form drag and/or gradients of field variables (temperature, velocity) are present, the analogy is conventionally known to be invalid. Therefore, other analytical corrections need to be adopted.
An example is given by the so called "Chilton-Colburn analogy":

$$Re\frac{f}{2} = Nu \cdot Pr^{\frac{-1}{3}}; \tag{2.31}$$

This equation it is valid for $0.6 \leq$ Pr ≥ 60, for both laminar and turbulent flows.

2.6 Jet flows

A jet flow is created every time a certain mass of fluid is ejected trough a nozzle. Jets, such as wakes, belong to the so called "free flows". They differ from the so called "confined flows" (channel flows or boundary-layer flows) because their velocity profiles present two inflectional points[14]. As a consequence, these flows become highly unstable and immediately try to reach another equilibrium condition, but stable. If the flow reaches some kind of intermediate equilibrium condition, then condensates into vortices; otherwise it becomes turbulent. Types and position of these vortices depend on the disturbances that are inside the system that generates the jet. Also the environment affects the jet, as asserted by Hussein et al [15]. For this reason, jets behave like an amplifier of the disturbances, and it is a domain that is convectively unstable: modifying the disturbances, it is possible to modify the jet's flow topology.
Therefore, jets are highly controllable if disturbances can be accurately controlled; on the other hand, this makes the definition of an analytical model quite difficult. Indeed, since jets are highly affected by disturbances, each jet is different from the other: there is no universal jet.

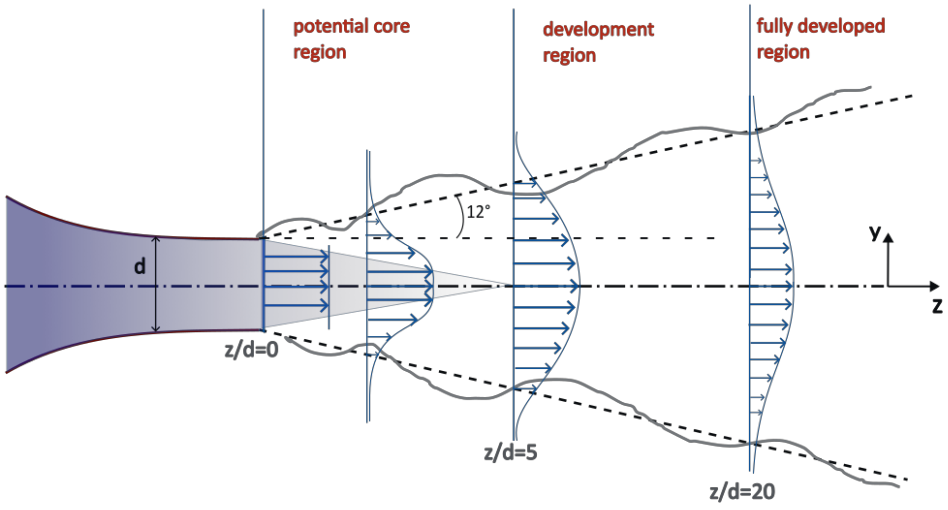

Figure 2.5: Topology of a jet flow[16].

We can separate the flow topology after the jet's exit into several regions [17]:

- An initial area where a shear layer forms, characterized by a top-hat velocity profile. This happens because of a very strong velocity gradient is present at the exit of the jet: indeed, the air with velocity equal to U_{jet} clashes with the still ambient air.After the shear layer formation, it develops in the streamwise direction;

- As the shear layer develops downstream, the potential core region is progressively replaced. This continues up to a distance of about 6 jet's diameter, in which the core region has disappeared;

- From 6 to 20 characteristic lengths, there is the so called development region, in which the mean streamwise velocity profile keeps changing;

- After about 20 characteristic dimensions, begins the so called "fully developed region", or self-similar region . Here, the velocity profiles assume a shape that preserves itself in the streamwise direction. Indeed, the velocity profiles assume the typical Gaussian shape.

2.7 Flow control with active system

Thermal engineers use a variety of tools to control the convective heat flow within an application or system. Nowadays, the two main solutions for heat transfer enhancement in wall-bounded flows are either passive or active methods.

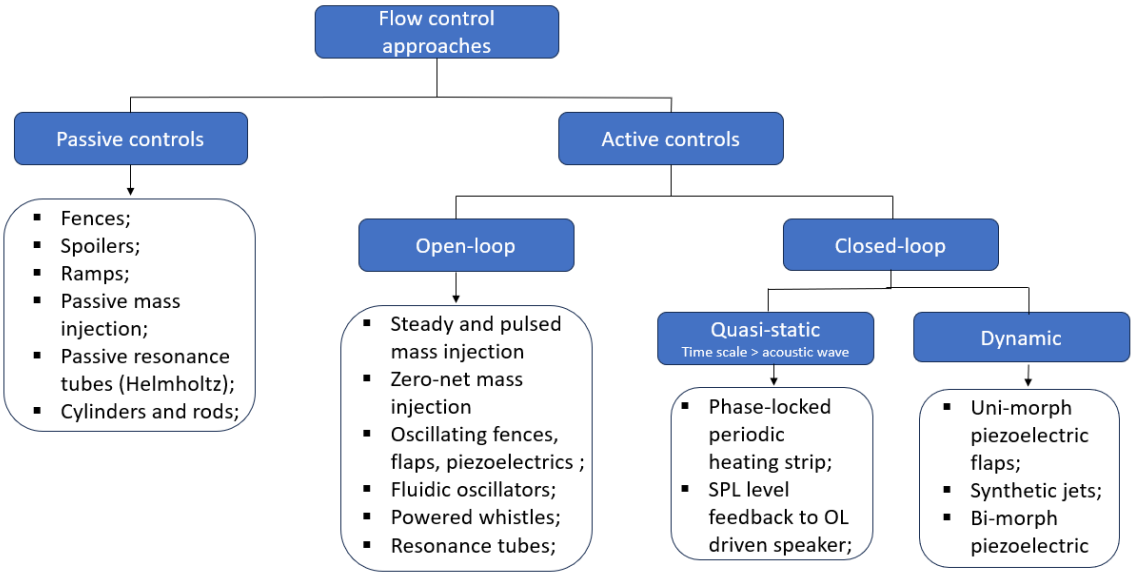

Figure 2.6: Active and passive methods[18].

Both of them aim at producing embedded streamwise vortices in the boundary layer, in order to improve the momentum transfer and/or the convective heat transfer within the boundary layer [19].
In this project, it is used an active method, that is an impinging jet in cross-flow: by exciting the structure and the organization of large scale turbulence, an enhancement in convection capabilities is obtained, as demonstrated by Kataoka et al. [20].
In particular, the overall aim of this work is reproducing the experiment performed by Castellanos et al. [4], but at a much higher frictional Reynolds number, by using the CICLoPE wind tunnel. Nonetheless, other differences from the previous mentioned experiments are present: it is used a rectangular jet instead of a circular one, and the jet that is used in this project is transversal with respect to the cross-flow.

Liu and Sullivan [21] and Mladin and D. Zumbrunnen [22], report that adding pulsation to an impinging jet can both reduce or improve the heat transfer capability, depending on the actuation frequency: pulsating the flow at the jet's natural frequency promotes the formation of small eddies which enhance local heat transfer.

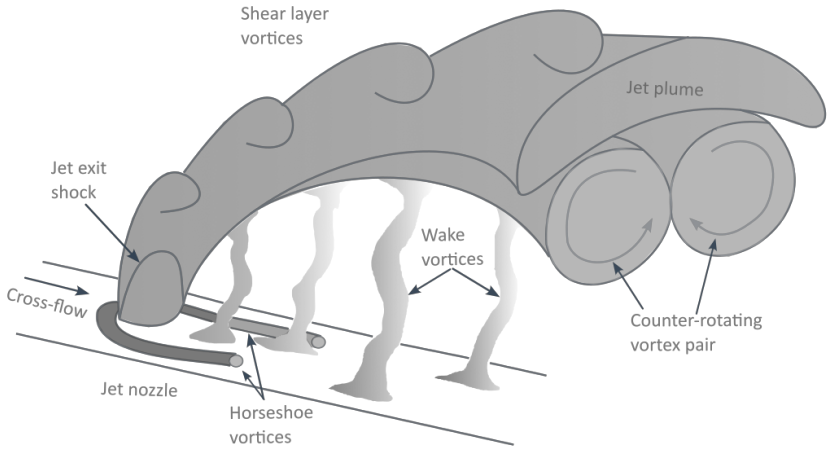

Figure 2.7: Vortex structure of a jet in cross flow.[23]

Similarly, Johari et al. [24] studied the mixing properties of fully-modulated (valve-actuated) turbulent jets in crossflow. It was found that both the frequency and duty cycle of the actuation influences the mixing properties, demonstrating that a short injection time provides a higher improvement of mixing and dilution compared to long injection times which resemble more closely steady jets.
Eroglu and Breidenthal [25] focused on the induced alterations on the vortical structures by the jet pulsation, finding that jets excited by square waves generate distinct vortex rings with up to 70% increase in penetration in comparison to steadily-blowing jets.
In particular, active flow control methods are very interesting, since they can be adapted to the changing conditions that may be faced in many practical applications. The active method shown in this thesis is a transverse jet in cross-flow: it is characterised by a counter-rotating vortex pair that forms downstream of the jet.
According to Fric and Roshko [26], four types of coherent turbulent structures are

present in the near field of the jet, shown in Figure 2.7:

- shear-layer vortices which dominate the initial portion of the jet;
- a system of horseshoe vortices that wrap around the base of the jet;
- the counter-rotating vortex pair (CVP);
- the wake vortices extending from the wall to the jet.

The formation and interaction among the coherent structures themselves and with the main flow have been widely studied and associated with the enhanced mixing efficiency of cross-flow jets.
Although most of the studies on jets in cross-flow are focused on round jets, there are several contributions (see e.g. [27], [28]) describing that the coherent structures and mixing characteristics are not greatly affected by the shape of the injected jet, especially in the far-field region of the flow. Furthermore, localised uniform blowing through a spanwise slot in the Turbulent Boundary Layer has also been investigated both experimentally and numerically.
One method in order to increase the transports of JICF is adding pulsation to the jet: both the frequency and the duty cycle of the jet influence the mixing properties. It has been shown that short injection times(short duty cycles) provide an improvement in mixing. Thus, the DC is the main promoter of the jet penetration; apart from modifying the intensity of the velocity field, the DC also alters the peak position, shifting it downstream for increasing duty cycle values.
Broadwell and Breidenthal [29] asserts that the jet mixing rate depends on the velocity ratio between the cross-flow and the jet, as it influences the penetration and bend of the injected flow. The velocity ratio also determines the extention of the wake region formed on the lee of the jet, where small velocity gradients and lower mixing are present [30] . Likewise, Smith and Mungal [31] affirm that this mixing enhancement is limited to the near field region of the flow, in which the formation of the CVP is dominant, and not to the far-field region where the CVP is completely developed.

Therefore, by varying frequency, duty cycle and velocity at the exit of the pulsed slot jet, an effect on the convective heat transfer must be present.
As a matter of fact, in the experiment of Castellanos et al. [4] they find out that the best absolute performance happens to be for a duty cycle of 75% and a pulsation frequency of 225 Hz. But including the volumetric flow rate in the estimation of the efficiency, the best control action is the one with the lowest duty cycle. This happens because the duty cycle is strictly related with the injected mass of fluid. Furthermore, a non-linear dependence of the Nusselt number with the pulsation frequency has been highlighted.
It is very interesting to point out that the efficiency of the actuation systems is rarely investigated. As a matter of fact, the initial approach is to find optimal solutions for the heat transfer enhancement.
A further step will be to estimate the cost in terms of the energy required by the actuation system, and comparing it with the gain in the energy-transfer enhancement.

The aim of this internship is to create the experimental setup that is able to generate a pulsed jet, and to control pulsation frequency, duty cycle and output velocity as input parameters.

Chapter 3

Experimental background

3.1 Experimental facility: the CICLoPE laboratory

As pointed out before, most of the experiments regarding the validity of control actions aimed at increasing the heat transfer have been performed at low frictional Reynolds number. This is also the case for the experiment of Castellanos et al[4].

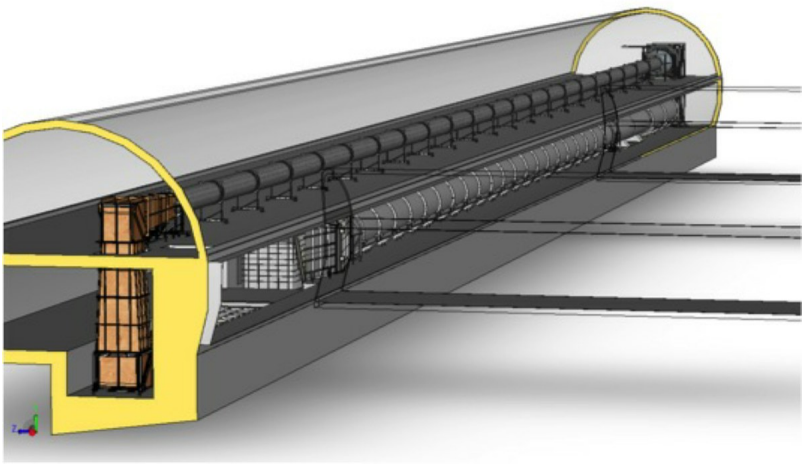

Figure 3.1: Schematic of the CICLoPE facility.[32]

3.1.1 Facility description

The CICLoPE laboratory, which stands for Centre for International Cooperation in Long Pipe Experiments, allows to study high Reynolds number turbulent flows. In particular, it is the research facility that allows to reach the highest Re_τ value, ranging from about 13300 up to 45000.

Frictional Reynolds number are a form of Re number based on the friction velocity u_τ:

$$Re_\tau = \frac{\delta\, u_\tau}{\nu}, \;\; where \;\; u_\tau = \sqrt{\frac{\tau_w}{\rho}}; \tag{3.1}$$

where δ is the characteristic dimension of the pipe, that is its radius, and τ_w represents the wall shear stresses. The importance of reaching such a high Re_τ lies in the fact that it allows to perform high resolution measurements even with "convenctional" measurement techniques, such as hot-wire anemometry.
As already discussed in Section 2.4, a very important parameter for the prediction of the skin friction of a turbulent flow is the " von Kármán constant", i.e. K. As a matter of fact, the following relation is valid:

$$C_f = 2\left(\frac{1}{K} ln\; Re_\tau + C\right)^{-2}; \tag{3.2}$$

where C_f is the skin friction coefficient. But in order to accurately determine the value of k, there is the need of sampling at least two points belonging to the overlap layer, which generally extends from $100 \leq y^+ \geq 0.15$ R.

It is now clear that, by increasing the Reynolds number, the viscous length scale becomes smaller and smaller, which in turn increases the value of y^+. This means that, as the Reynolds increases, the overlap layer enlarges and distances itself from the wall. This distancing from the the wall is sufficient enough to allow velocity sampling with a hot-wire anemometer.
As a matter of fact, for conventional high Re facilities, the overlap region does not expand by a sufficient amount to allow hot-wire anemometry velocity measurement. Conversely, in the CICLoPE wind tunnel, hot-wires can be safely used, bringing all the advantages of such a velocity measurement technique (high frequency response,

high spatial resolution).
Moreover, due to the peculiar site of the laboratory, the effect of external disturbances on the measurements is very low: this guarantees a high degree of repeatability of the experiments.

3.1.2 Long Pipe overview

Table 3.1: Long Pipe features.

Total length	120 m
Pipe length	111.5 m
Diameter	0.9 m ± 0.1 mm
Inner surface roughness	< 0.21 µm
Max speed	60 m/s
Fan power	380 kW
Temperature variation	$< \pm 0.1$°C
Test section length	1.5 m

The CICLoPE Long Pipe belongs to the category of closed-loop wind tunnels operating with air at ambient pressure. Indeed, a closed-loop design offers the possibility to accurately control the flow characteristics such as velocity, temperature and humidity. The main components are:

- The test section. It is the most important part, from a preliminary design point of view, because it can be the source of many undesired effects(blockage effects). It can be easily removed and replaced by a custom made to meet different experimental requirements;

- The effuser. Characterized by its contraction ratio, it accelerates the flow by creating a Favourable Pressure Gradient, and reduces the turbulence intensity;

- The settling chamber. Inside this section, screens and honeycombs are placed in order to align the flow with the streamwise direction and to eliminate large scales vortices;

- The diffuser. It creates an Adverse Pressure Gradient by slowing down the flow, hopefully without separation. It is used in order to recover as much static pressure as possible, and it is characterized by the opening angle;
- The driving unit. It must both produce the pressure drop to overcome, and provide the necessary flow rate to originate the flow needed in the test section;
- The cooling system. It is used in order to keep the temperature inside the test section as constant as possible.

3.1.3 Need for customized parts

The effectiveness of the active flow control on the heat transfer enhancement has to be measured at the wall. Therefore over the PCB a uniform cross-flow must be present. For normal experiments which require to insert some kind of object attached to the wall, a particular pothole has been design.

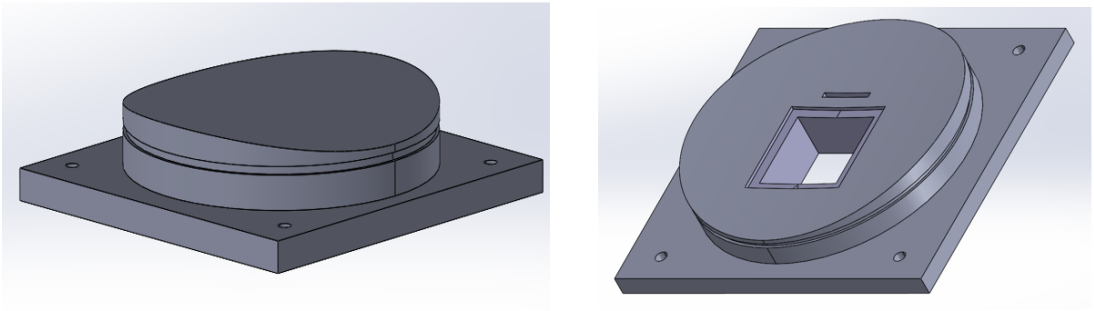

Figure 3.2: The particular pothole for the wind tunnel. On the left, the standard configuration; on the right, the configuration adopted for these experiments.[32]

The pothole on the left is the standard configuration of the pothole: it is designed to fit with the internal curvature of the wind tunnel, therefore its curvature radius is 450 mm. This piece is fixed from the outside with 4 screws, and its height is carefully selected to avoid the creation of steps inside the test section.

For this particular experiment, this pothole was not made of steel, but has been manufactured with a 3-D printer: the material was the PLA (PolyLactic Acid). To avoid any impurity and to increase the surface roughness, the top of the pothole has been finished with sandpaper. In addiction, the geometry has been modified so to accommodate the slotted jet and the PCB board.

3.2 Hot-Wire anemometry

During the experimental campaigns, the acquisition of the velocity signal was performed by using a hot-wire anemometer. This kind of instrumentation needs to be calibrated, in order to uniquely relate a voltage value to a predefined velocity value. The velocity value is acquired by using a static-Pitot tube, throughout differential pressure measurements.
An anemometer is a device that is capable of measuring the velocity of the air of the impinging flow. The hot-wire is a thermal transducer, that is a device that transforms a temperature variation into an electric signal.

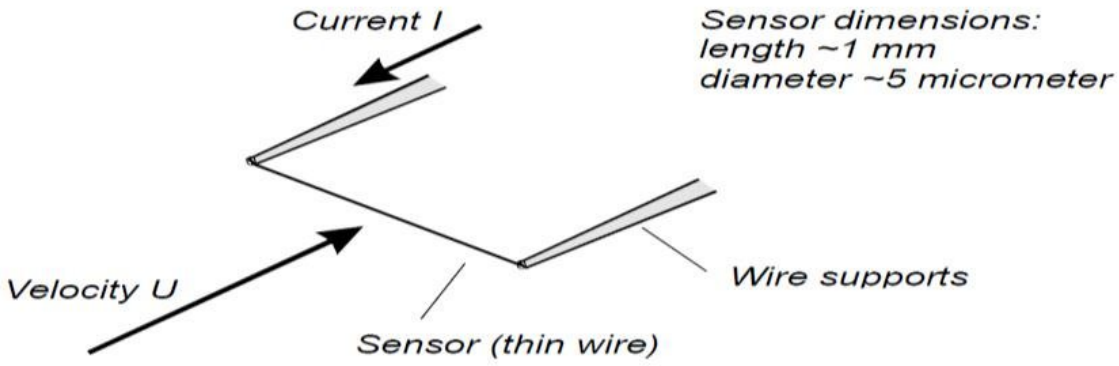

Figure 3.3: Scheme of a hot-wire probe.[33]

Indeed, its working principle can be summarized as follows: a fine current-carrying filament exposed to a cross flow experiences a cooling effect. This modifies the resistance of the wire(the sensing element), which is expressly made of particular materials with a high temperature coefficient of resistance(platinum, tungsten).

This change in the resistance of the hot-wire's filament is measured by an electronic device which contains a Wheatstone-bridge circuit.
The cooling effect is mainly associated to forced convection heat losses, which are strongly velocity dependant, but other effects such as diffusion, heat conduction to wire supports and radiation contribute to the heat balance of the filament[34]. Therefore, only after a calibration procedure, it is possible to quantify the velocity of the impinging flow.
Hot-wire anemometers are very widespread in turbulent flow measurements, because offer many advantages of other measurement techniques. As an example, if compared to LDA of PIV, they present a much lower cost, an extremely good spatial resolution and a frequency response (unfiltered) up to 50 kHz, compared to 30 kHz of LDV.
On the other hand, several problems are present:

- They are intrusive methods: since they need to be in contact with the flow, the supports and also the wire itself alter the flow;
- They need frequent calibration procedures: this is due to the fact that are very sensitive to variations of ambient parameters and may be affected by contamination;
- They are delicate: because of the very small dimensions of the wire (few micrometers), even some small impact can seriously compromise its working;
- Their use is limited to low and medium intensity turbulent flow: indeed, high turbulence levels may cause reverse flow, leading to unphysical results.

3.2.1 Operating modes

The hot-wire anemometer can operate according to two different modes:

- Constant Current Anemometer(CCA). In this application, the current through the wire is kept constant. Therefore, once a specific overheat ratio has been selected, the Wheatstone bridge is kept in balance by acting on the cable resistance and on an adjustable resistance.

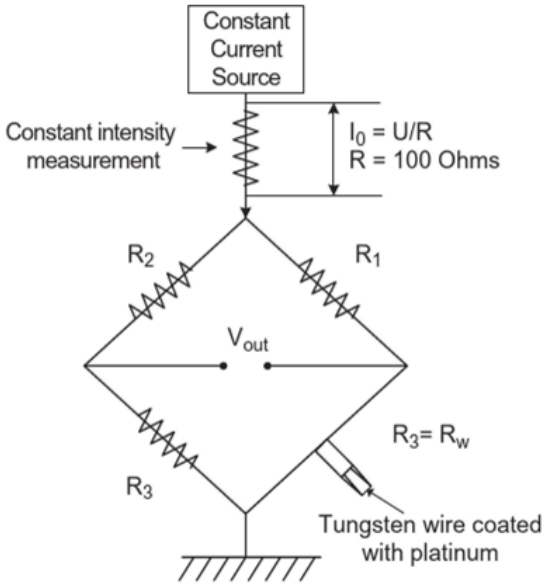

Figure 3.4: Constant Current Anemometer scheme[33].

Accordingly to this, due to a resistance variation caused by a wire temperature variation, the Wheatstone Bridge calculates the voltage variation required to maintain that value of current. This is the very first operating mode, from a historical point of view.

- Constant Temperature Anemometer(CTA). In this application, the temperature of the wire is kept constant, by varying the current thanks to a feedback loop. Therefore, as the temperature of the wire changes due to forced convection, the feedback loop changes the current.

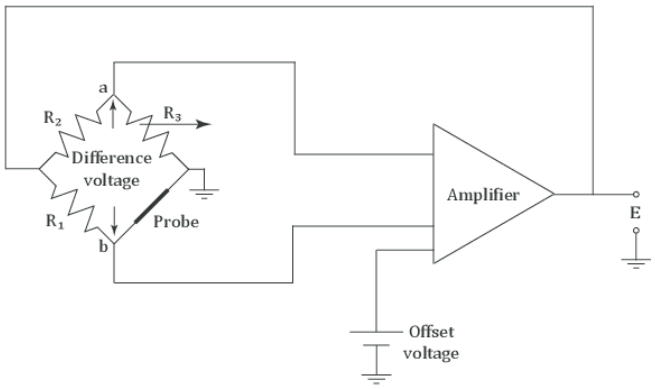

Figure 3.5: Constant Temperature Anemometer scheme[33].

A very crucial role is played by the thermal inertia of the hot-wire filament. As a matter of fact, the Wheatstone bridge determines the voltage difference based on a temperature variation of the wire and due to the thermal inertia, the temperature settlement requires a certain amount of time. This limits the frequency response of CCA, which however is still used for temperature measurements.
On the other hand with CTA the problem of the thermal inertia is easily overcame, because the temperature is kept at a constant value. Therefore, the frequency response of a CTA is much larger than CCA, because is only determined by the electronics of the feedback loop. The problem was that such a system has an untable behaviour, but nowadays this is not an issue anymore: therefore, nowadays CTA is the operating mode universally adopted for turbulent velocity measurements.

3.2.2 The Nusselt number

The Nusselt number expresses, in a non-dimensional form, the convective heat transfer coefficient: therefore, for a cylinder, is written as:

$$Nu = \frac{h \cdot d_w}{k_f}; \tag{3.3}$$

where k_f is the thermal conductivity of the fluid and d_w is the wire's diameter. In general, the Nusselt number is a function of many parameters:

$$Nu = Nu\left(M, Re, Gr, Pr, \gamma, \frac{T_w - T_a}{T_a}\right); \tag{3.4}$$

where:

- $M = \frac{U}{c}$ is the Mach number;
- $Re = Re_w = \frac{U d_w}{\nu}$ is the Reynolds number referred to the diameter of the hot-wire;
- $Gr = g \cdot \beta\,(T_w - T_a)\,{d_w}^3\nu^2$ is the Grashof number and expresses the ratio of the buoyancy to viscous forces;
- $Pr = \frac{c_p \nu}{c k_f \rho}$ is the Prandtl number, which expresses the ratio of momentum diffusivity to thermal diffusivity.

These parameters represent, respectively: the Mach, Reynolds, Grashof and Prandtl numbers, the ratio between specific heat at constant pressure and volume, and the wire temperature difference. But considering that the effects due to natural convection can be neglected and the flow as incompressible, Equation 3.4 reduces to:

$$Nu = Nu\left(Re_w, \frac{T_w - T_a}{T_a}\right); \tag{3.5}$$

Since the wire diameter is a constant, the Re_w only depends on the free stream velocity U, therefore it can expressed as:

$$Nu = A_1 + B_1 U^n; \tag{3.6}$$

where usually n= 0.5. Furthermore, by combining other equations to Equation 3.6, the result is the so called King's law:

$$\frac{I_w^2 R_w}{R_w - R_a} = A + BU^n; \tag{3.7}$$

Finally, by expressing as V_w as the product between I_w and R_w, the voltage across the hot-wire can be written as:

$$V_w^2 = A + BU^n; \tag{3.8}$$

3.2.3 Calibration procedure

The calibration procedure of a hot-wire anemometer is used in order to establish the relationship between the anemometer output voltage and the magnitude of the incident velocity vector.
For the calibration procedure, a Planar Air Tunnel (PAT) has been used. It is a planar wind tunnel specifically developed for the calibration of hot-wire probes. The anemometer is placed at the exit of the jet of the PAT, which is operated at different velocities: the output is a set of voltage value whose values increase as the velocity does.
To each voltage value it is associated a velocity value, which is obtained by a static-Pitot probe (or Prandtl probe). A static Pitot tube is a device that provide the value of the static and total pressure, whose value is measured by two pressure transducers. Applying the Bernoulli's equation between the two points in which the two pressures are measured, the following equation is obtained:

$$V1 = \sqrt{\frac{2\,(p_0 - p_1)}{\rho}}. \tag{3.9}$$

where p_0 represents the total pressure and p_1 represents the static pressure.
It is very important to clarify one point: since 3.9 derives from Bernoulli's equation, that equation can only be applied to incompressible flows. As a matter of fact, only for incompressible flows the difference between total and static pressure is the so called "*dynamic pressure*". When dealing with compressible flows this relationship is no longer valid and therefore equation 3.9 has to be modified.
Finally, a calibration curve must be fitted to these calibration points according to predetermined calibration curves, such as the King's law (3.8) or a polynomial curve:

$$U = A_0 + A_1 V_w + A_2 V_w^2 + A_3 V_w^3 + A_4 V_w^4; \tag{3.10}$$

The result of this interpolation procedure are the calibration coefficients, which allows to relate every voltage value measured by the hot-wire to a velocity value.

3.2.4 Temperature correction

Especially for the case of the spanwise velocity profile's acquisitions, the duration of the whole experiment was considerably long. Due to the floods occurred in Predappio, the experiments have been moved to a completely different location with respect to the underground laboratory. The new location was inside a structure with glass walls, and characterized by a severe temperature increase due to the solar exposition. An air conditioning system was present, but in any case the temperature cannot be considered constant anymore. This is shown in Figure 3.6:

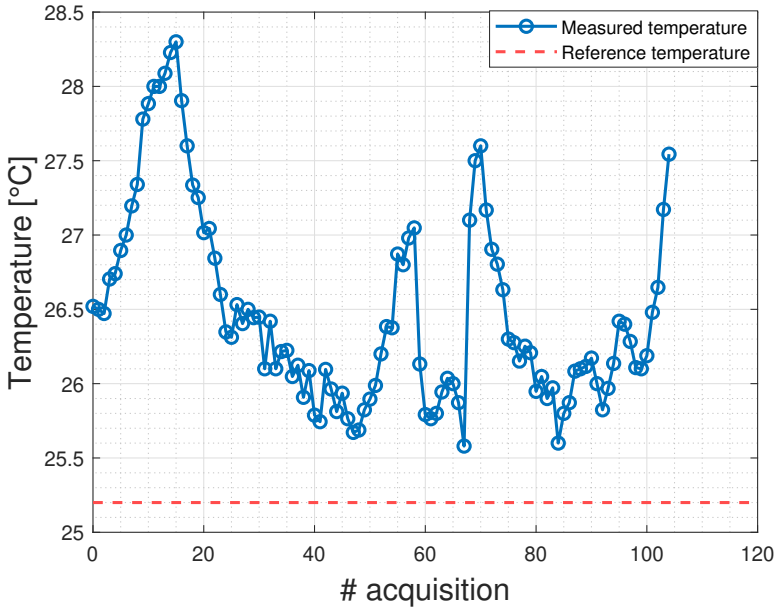

Figure 3.6: Temperature variation during one single experiment.

These temperature values are measured with a thermocouple PT100: at the end

of each acquisition, a set of 25 temperature values were acquired, and then the mean value has been taken as the reference temperature. Finally, the temperature correction has been performed, according to the formula in 3.11:

$$V_{corr} = \frac{V_i}{\sqrt{1 - \frac{T_i - T_{ref}}{\alpha_t / \alpha_r}}} \tag{3.11}$$

, where:

- V_{corr} is the voltage after the temperature correction;
- V_i is the voltage before the temperature correction;
- T_i is the temperature of the single experiment;
- T_{ref} is the calibration temperature;
- α_t is the overheat ratio, $\alpha_t = 0.8$;
- α_r represents the electrical resistivity, $\alpha_r = 0.0036$;

The results after the temperature correction are shown in Figure 3.7:

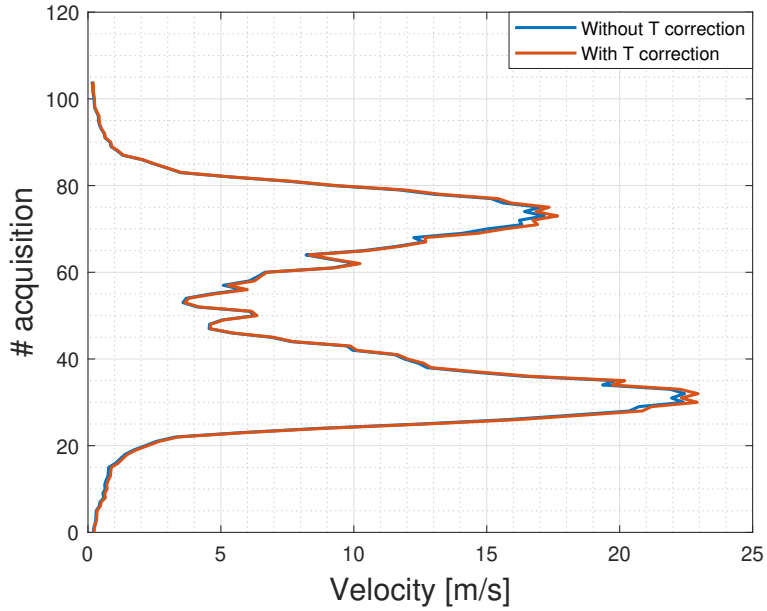

Figure 3.7: Differences in the velocity profile due to the temperature correction.

As expected, the difference in the velocity values can be appreciated only in those regions where the temperature difference becomes larger than 3 °C.

Chapter 4

Experimental setup

In this chapter, an explanation of the principles behind the acquisition procedure is carried out. Subsequently, it is presented the instrumentation that has been used for the validation of the active flow control, with their own specifications.

4.1 Hardware setup

For this thesis, the following hardware setup has been used:

1. One compressed air treatment unit;
2. One pressure regulator;
3. One mass flow rate sensor Honeywell HAFUHT0200L4AXT;
4. One electronic circuit controller;
5. One solenoidal valve SMC SX12F-DH;
6. One 3-D printed pothole;
7. One slotted jet;
8. One hot-wire anemometer;

9. One compact-RIO board NI cRIO-9068 with different modules;
10. One compact-DAQ board NI cDAQ-9189 with different modules;
11. Three power supplies;
12. One pressure measurement system;
13. One stepper motor;
14. One Arduino Uno microcontroller;
15. One Dantec StreamLine 90N10;
16. One thermocouple PT100;
17. A computer with NI LabView.

A sketch of the setup is shown in Figure 4.1:

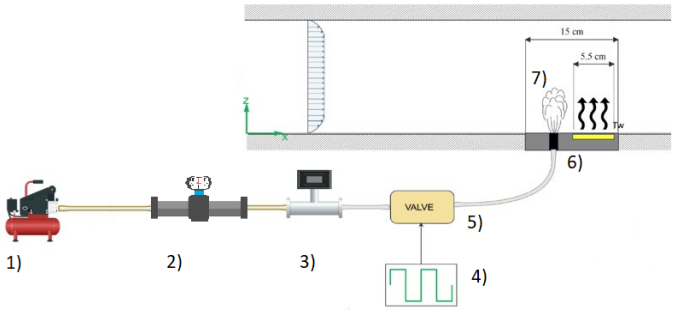

Figure 4.1: Schematic of the hardware setup. Courtesy of A.Gessi.

4.1.1 Jet's specifications and optimization

The jet adopted in this thesis work is the one proposed by Castellanos et al.[4]. It injects the air in the turbulent boundary layer, and it is equipped with vanes to

improve the flow uniformity across the slot width and to reduce the pressure losses within the final part of the slotted jet.

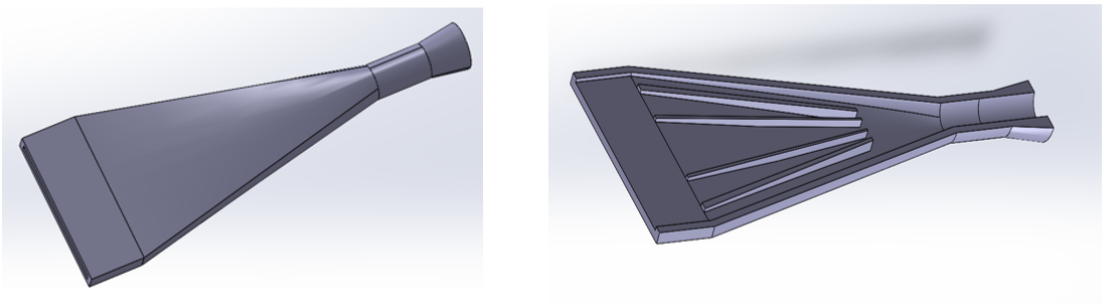

Figure 4.2: The jet's geometry (on the left). On the right, a section view to highlight the guide vanes.

The design of the actual jet it is shown in Figure 4.3, and composes as follows:

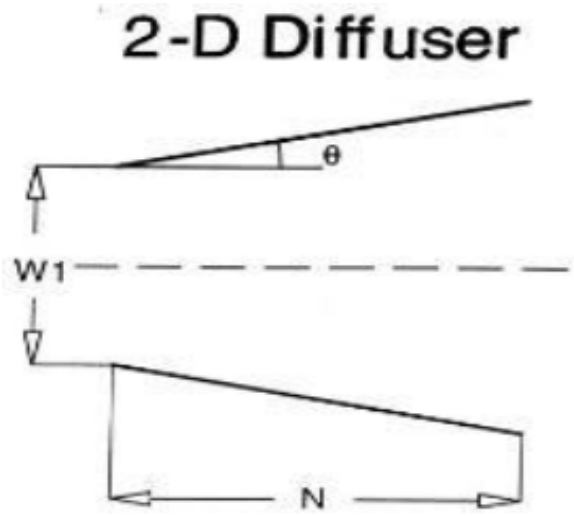

Figure 4.3: Schematic of a 2-D diffuser.

- N= 49.5 mm;
- W1= 3.96 mm;

- θ= 11.86 °;
- Presence of guide vanes for flow homogenization.

Considering the following parameters, the jet is characterized by N/W1=12.5 and by 2θ=24 °. Therefore, according to the graph shown in Figure 4.4, it is in a regime of large transitory stall(red point).

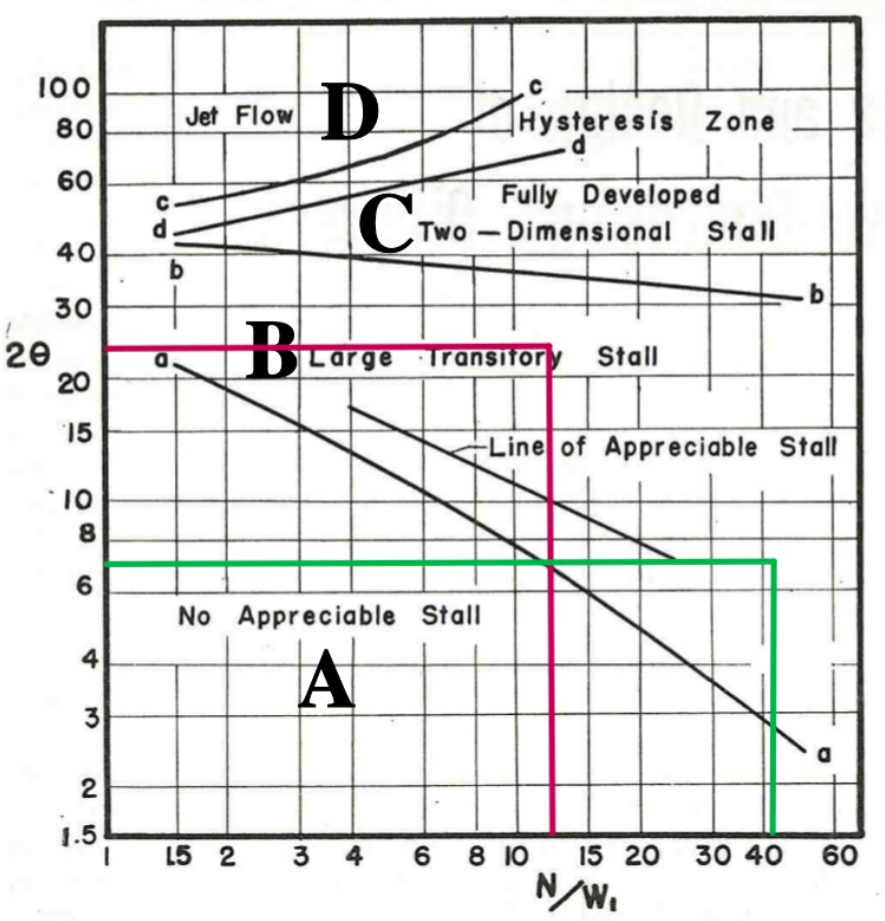

Figure 4.4: Regime table for a 2-D diffuser[35].

This jet is flush-mounted into a 3-D printed pothole, especially developed for the application in the CICLoPE wind tunnel.

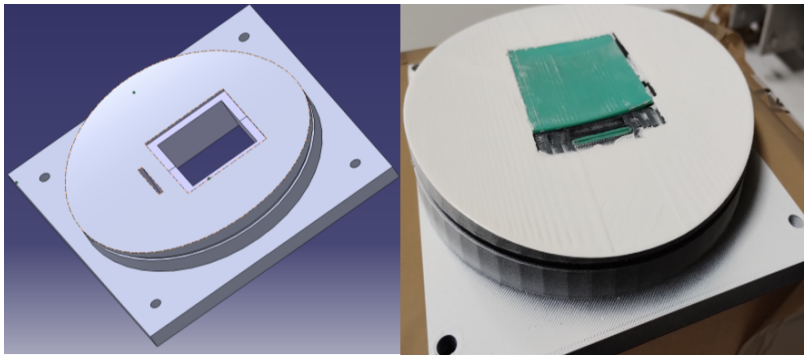

Figure 4.5: The 3-D printed pothole.

At the center of this component there is the slot for the successive insertion of a Printed Circuit Board (PCB). It is a very thin electronic circuit that will be used as a heating element to effectively assess the convective heat transfer enhancement.

4.1.2 Pneumatic circuit

The pneumatic circuit encloses all those instruments which generate and control the flow up to the solenoidal valve.
The compressor that has been used is the BLACK&DECKER - BXCM0031E, whose main characteristics are the followings:

Table 4.1: Air compressor features.

Electric supply (V/Hz)	230/50
Power (Hp)	2
Max operating pressure (bar)	8
Tank volume (L)	24
Suction capacity (L/min)	210

Then, a pressure regulator it is present: this filter allows to set the pressure value inside the pneumatic circuit. Furthermore, thanks to its filter, eliminates the majority of the water vapour which is present inside the ducts.

The next instrument is a mass-flow meter, the Honeywell- HAFUHT0200L4AXT: its main features are reported in table4.2 and Figure 4.6:

Figure 4.6: Mass-flow meter.[36]

This device is controlled by an Arduino-Uno board, and it is characterized by a quick response time, a high stability, a low sensitivity due to thermal effects and a high 12-bit resolution. The sensor uses the I2C standard for digital communication with a specific slave address. The first read after power-up will respond with the two most significant bytes of the Serial Number, while the second read will respond with the two least significant bytes of the Serial Number.
For reliable performance, it is recommended to allow the sensor to be powered for the sensor startup time before performing the first read, then allow a 10 ms command response time before performing the second read. Furthermore, the equation that it is adopted to calculate the flow rate is the following:

$$SLPM_{meas} = FS \cdot [(Counts/16384) - 0.1] / 0.8; \tag{4.1}$$

A schematic of the circuit is shown in Figure 4.7, while the main features of the mass-flow sensor are reported in 4.2:

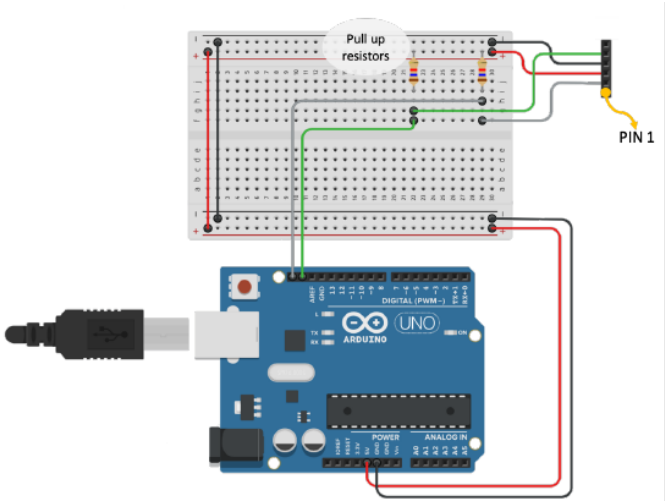

Figure 4.7: Electric circuit for the mass-flow sensor. Courtesy of A. Bragoni.

Table 4.2: Flow-rate sensor specifications.

Supply voltage	3 Vdc to 10 Vdc
Supply current	20 mA max
Operating temperature range	-20°C to 70°C
Full scale (FS) flow	200 SLPM
Flow response time	1 ms
Proof pressure	10.3 bar
Bus standards	I2C fast mode (up to 400 kHz)

4.1.3 Pressure measurement circuit

The pressure measurement circuit encloses all those instruments that have been exploited for the hot-wire calibration. As a matter of fact, for the hot-wire calibration two MKS Baratron 120AD pressure transducers were used, connected to the MKS PR4000B. The first pressure transducer had a pressure range of 10 Torr and was connected to the static-Pitot probe; the second one measures the ambient pressure, therefore requires a pressure range of 1000 Torr.

Figure 4.8: Baratron and MKS instruments.[37]

The 120AD Differential combines the proven 698 Baratron High Accuracy Sensor and 270 Signal Conditioning Electronics - oscillator, demodulator, and amplifier-within a single, chemically inert, injection-molded, high impact enclosure. The compact 120AD Differential can be powered by 24-30 VDC or ± 15 VDC, and has a high level 0-10 VDC output.
Standard features include a temperature-controlled sensor to 45 °C, a remotely activated range turn-down capability to provide Full Scale output of 0-10 Volts for 100% and 10% of sensor range, and a remote automatic zeroing capability up to ±2% of Full Scale.
As a matter of fact, in order to increase the accuracy of the instrument, the transducers are enclosed into a 45 °C ambient: so doing, temperature changes of the ambient do not affect the pressure.

4.1.4 The electronic circuit

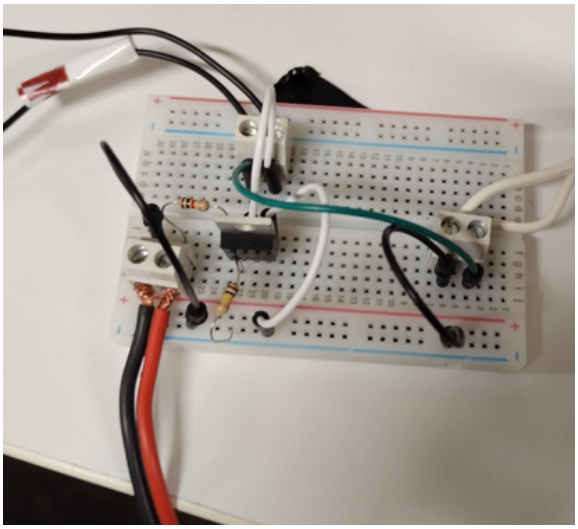

Figure 4.9: The electronic circuit.

The electronic circuit has been developed to create the pulsed signal that must control the solenoidal valve, that is the square wave signal. It composes as follows:

- A 24 VDC power supplier;
- The NI-9263 module connected to the cDAQ;
- A mosfet IRFZ-44N;
- Two resistors of 1 kω and 10 kω.
- The solenoidal valve.

It works as follows: the c-DAQ 9189 and the module NI-9263 generate a square wave signal from 0 to 6 VDC. This signal triggers the mosfet IRFZ-44N, which acts as a switch that, coupled with a constant 24 VDC signal coming from the power supply, generates a square wave signal ranging from 0 to 24 VDC. As a matter of fact, the solenoidal valve requires 24 VDC as input.

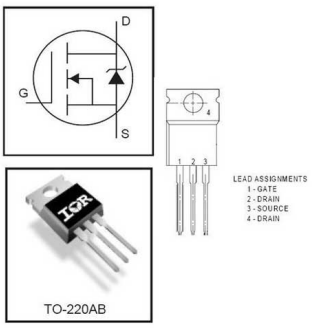

Figure 4.10: The mosfet IRFZ-44N.

A mosfet is an electronic component characterized by 3 main terminals with terminals: source (S), gate (G), drain (D). Its working principle is relatively simple: when the voltage between the gate and the source is lower than the threshold voltage ($V_{GS} < V_{TH}$), the Mosfet works as a switch in "OFF" position. On the contrary, when the voltage between the gate and the source is higher than the threshold voltage, the Mosfet works as switch in "ON" position. Table 4.3 reports some specifications about the mosfet:

Table 4.3: Mosfet IRFZ-44N specifications.

Type of Control Channel	N -Channel
Maximum Power Dissipation (Pd)	150 W
Maximum Drain-Source Voltage (V_{DS})	60 V
Gate-to-Source Voltage (V_{GS})	± 20 V
Rise Time	110 ns

4.1.5 Printed Circuit Board

A printed circuit board, or PCB, is a non-conductive material with conductive lines printed or etched. In the usual conditions they are employed in order to connect several electronic circuits to form a working circuit. But in this thesis, it has been used as a heating source for the creation of a specific thermal gradient.

Indeed, we want to create a temperature difference of about 10 °C between the temperature of the wall T_w and the temperature of the flow (T_∞ = 20 °C).

Table 4.4: PCB specifications.

Input parameters	
Track's material	Copper
Width of the tracks	18 µm
gap between tracks	0.2 mm
Width of PCB	250 µm
Dimensions of the PCB	55 x 55 mm
Material of the PCB	Flexible fiberglass

A very important parameter that must be evaluated when designing a PCB is the Biot number (Bi):

$$Bi = \frac{\overline{h}t}{\lambda}; \tag{4.2}$$

where:

- $\overline{h}$ is the mean convective heat transfer coefficient, and for this experiment it is equal to 93.3;
- t is the material thickness, t=0.25mm;
- λ is the thermal conductivity, which is equal to 400,25 $\frac{W}{mK}$ (copper + fiberglass).

Therefore, since the Biot number is much smaller than one (Bi= 5.8 10^{-5}), thermal gradients across the thickness of the heat-flux sensor can be considered negligible

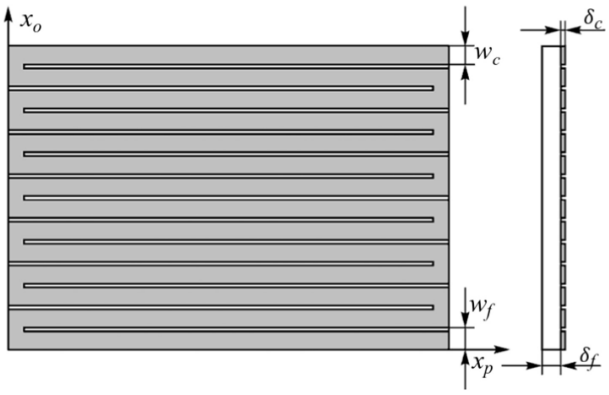

Figure 4.11: Schematic of a PCB.[38]

A feasibility study is carried out by rewriting the energy balance at the PCB surface: the input heat is the one generated by the Joule effect (q_j). On the other hand, the outgoing heat encloses several contributions. Neglecting the conductive heat flux from the surface of the sensor to the support, we can write:

$$q_j = q_c + q_r + 2q_{ktan}; \tag{4.3}$$

where:

- q_c is the convective heat flux from the heater to the flowing fluid;
- q_r is the heat flux by radiation;
- q_{ktan} is the conductive heat flux from the 4 ends of the sensor that are in contact with the support.

A more detailed explanation about all the contributions on the right hand side of 4.3 are discussed in [4]. Recalling that $q_j = \frac{VI}{A}$, it is therefore possible to estimate the electrical quantities needed maintain the necessary temperature.

4.1.6 The solenoidal valve

The solenoidal valve SMC SX12F-DH is the high-speed actuator for the square wave signal generated by the electronic circuit.

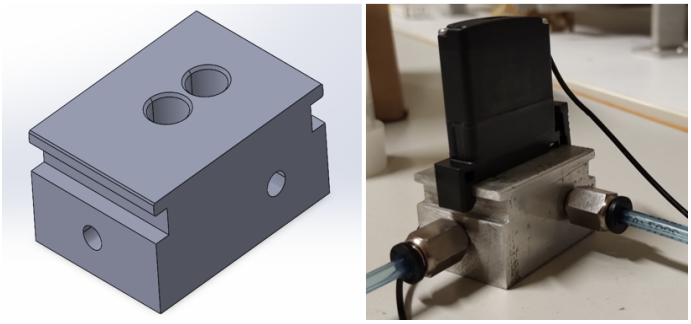

Figure 4.12: The solenoidal valve, with its hand-made support.

Solenoid valves are control units which, when electrically energized or de-energized, either shut off or allow fluid to flow. The actuator takes the form of an electromagnet: when energized, a magnetic field builds up which pulls a plunger or pivoted armature against the action of a spring. When de-energized, the plunger or pivoted armature is returned to its original position by the spring action.
The main features are described in Table 4.5:

Table 4.5: Solenoidal valve specifications.

Switching type	Normally closed
Flow rate	50 L/min
Power Consumption	4 W
Maximum operating frequency	350 Hz
Maximum operating pressure	6 bar
Fluid operating temperature	- 10 °C to 50 °C
Opening response time (at 2.5 bar)	1.25 ms
Closing response time (at 2.5 bar)	0.4 ms

The values of the delay time in the opening and closing phase are very important, in particular for high values of pulsation frequency. As a matter of fact, SMC

company infers that both the response time and the maximum operating frequencies are not guaranteed. This suggests to use a solenoidal valve which is certified for a higher maximum operating frequency.

Figure 4.13: Two types of the solenoidal valve: quick-disconnect (on the left) and screw-mount (on the right).[39]

Another important aspect that must be taken into account is the following: this valve has a quick-disconnect mount on its support; this mounting may cause air leakages. Therefore, a screw-mount type would be more appropriate.

4.1.7 Acquisition devices

When talking about Data Acquisition, commonly abbreviated as DAQ or DAS, one refers to the process of measuring physical phenomena and recording them, in order to analyze them. Typical DAQ systems integrate more than one conditioning channels that constitute an electrical interface circuit between the external sensor and the A/D conversion subsystem.
During the experiment, both c-DAQ 9189 and C-RIO 9068 acquisition boards have been used.

Figure 4.14: On the left a c-DAQ chassis; on the right, a c-RIO chassis.[40]

A c-DAQ system always consists of a controller or chassis and the modules installed in it. It is very easy to program and universally usable due to the large number of available modules, but it has not a real-time behavior and does not supports complex modules such as CAN bus interfaces.

A c-RIO system looks very similar to a c-DAQ, but the important difference lies in the fact that there is no passive BUS installed here, but a FPGA (hence the name "re-configurable"). A c-RIO system has different layers in which user-written software runs: the FPGA back-plane, the c-RIO controller and the application program in a PC. Lab-VIEW with additional tool-kits FPGA and Real-time allows to implement the code of all three levels. A c-RIO system can also work autonomously without a connected computer (measuring, controlling, regulating, recording).
Therefore, a c-RIO is more expensive than a c-DAQ, and programming much more complex (Lab-VIEW Real-Time and FPGA required). But on the other hand, it provides a real-time behaviour, can read more complex cards (such as CAN bus) and has a large availability of modules.
A field-programmable gate array (FPGA) is an integrated circuit designed to be configured after manufacturing. The FPGA configuration is generally specified using a hardware description language (HDL)and contain an array of programmable logic blocks, and a hierarchy of reconfigurable interconnects allowing blocks to be wired together. Logic blocks can be configured to perform complex combinational functions, or act as simple logic gates like AND and XOR. In most FPGAs, logic

blocks also include memory elements.

Figure 4.15: Example of NI modules.[40]

During all the experiments, the following modules were used:

- NI-9263: is the module chosen to control the solenoidal valve.This is the module used for the creation and control of the parameters of the square wave signal. As output it generates an analogue wave,and the module is compatible with LabVIEW and the chassis NI c-DAQ 9189. This signal is acquired and analysed, since it is the reference signal that triggers the solenoidal valve[40].

- NI-9401 and NI-9501 : both of these modules are employed to operate the stepper motor with the c-RIO chassis. The NI-9401 is a digital I/O interface for input or output in 4-bit increments. NI-9501 C Series Motor Drive Module can be utilized with 2-phase hybrid stepper motors in bipolar or unipolar winding configuration. The NI-9501 utilizes an advanced PWM algorithm that minimizes torque ripple, reduces emissions, lowers power loss, and generates a smoother motion throughout microstepping[40].

- NI-9215:it is used for the acquisition of the analogue inputs that come from the hot-wire and the square wave signal generator. As a matter of fact the NI

9215 is an analog input module for use with NI Compact-DAQ and Compact-RIO systems. The NI 9215 includes four simultaneously sampled analog input channels and successive approximation register (SAR) 16-bit analog-to-digital converters (ADC). It also contains a channel-to-earth ground double isolation barrier for safety and noise immunity, and high common-mode voltage range[40].

Finally, the hot-wire is operated through a Dantec StreamLine 90N10 frame with 90C10 CTA modules: since a single-wire probe was used, it was necessary one single CTA module. The CTA modules have a Signal Conditioner that is used to match the CTA bridge output voltage to the input range of the A/D converter board in the PC and also to perform filtering of the signal. It can be operated in both DC and AC mode.
It contains an input Offset circuit that subtracts up to 10 Volts from the bridge output voltage with a resolution of 1 mV and a Gain function that amplifies the resulting signal up to 1024 times. The AC voltage signal from the CTA can be low-pass filtered (10 kHz) to reduce any high-frequency noise associated with the electronic circuitry. Furthermore, a high-pass filter of 10Hz can be used to remove any mean and low frequency components of signals before being digitized with a 12-bit A/D converter[41].

Figure 4.16: A StreamLine 90N10 with CTA modules 90C10.

4.1.8 Temperature probe

For this experiment, a PT100 temperature sensor was used, both for the hot-wire calibration and for the monitoring of the temperature during a whole experimental campaign. The PT100 belongs to the so called RTD sensors (Resistance Temperature Detector), which exploit the change in the electrical resistance of metals in order to measure the change in local temperature.

Figure 4.17: A PT100 RTD sensor.

The main benefits of a RTD sensor is the good accuracy over a fairly wide range and combined with excellent stability, this is in contrast to a thermocouple which is less accurate, less stable and can drift over time. RTD sensors are more suitable for lower temperature ranges, where higher accuracy and repeatability is needed. They also need to be immersed in the media due to stem conduction errors.
A practical benefit of RTDs over thermocouples is that they use standard electrical wiring, where thermocouples require compensated alloys and connectors over the entire length up to the connection of the instrument. Here there are some features of a PT100 sensor:

Table 4.6: PT100 sensor specifications.

Typical temperature range	from -50 °C up to 300 °C.
Max temperature range	from -200 °C up to 850 °C.
Signal strength	High.
Self-heating	Yes.
Best for	Consistent readings.
Worst for	Surface readings.

4.2 Measurement chain

A measurement chain is the set of instruments and operations necessary to acquire and store any physical quantity of interest. A schematic is shown in Figure 4.18:

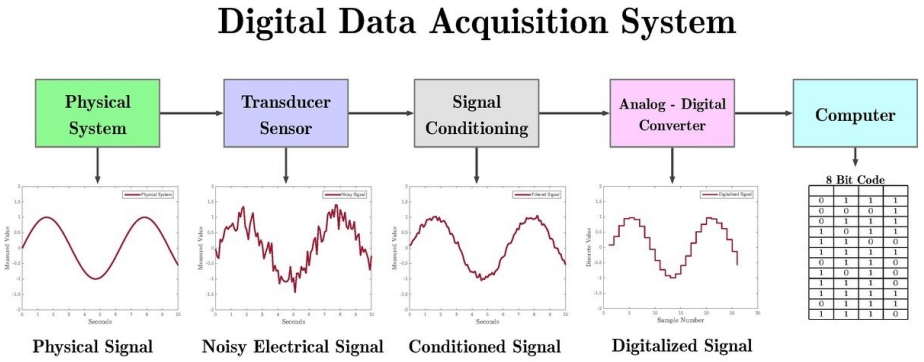

Figure 4.18: Schematic of a measurement chain.[42]

Almost every physical quantity of interest in aerodynamics can be represented as an analogue signal, therefore it must be converted into a digital signal. Many elements are present in the measurement chain:

- Sensors: they are the elements which change their status when "in contact" with the physical quantity to be measured.
- Transducers: they represent the element which transforms the changes in the sensor's status in an output "signal" by converting an energy form into another.

The typical output signal is an electric signal, but this is not said a priori; an example of a transducer is the Wheatstone bridge.

- Signal conditioners: such as filters or amplifiers. The signal conditioning operation manipulates the signal in order to make the acquisition process more efficient. Therefore, an amplification of the signal can be performed in order to improve the resolution. Or a filtering operation may be necessary: low-pass filters are usually adopted to avoid aliasing, while high-pass filtering is used for noise reduction.

- A/D converters: they are the devices that discretize the analogue signal into a digital one. A reference parameter is the Signal to Noise Ratio (SNR), which represents the ratio between the amplitude of the signal to be measured and the discretization error. In order to increase this parameter, it can either be increased the number of bits used to encode the analogue signal, or decreased the range of acquisition of the A/D converter.

Many parameters have to be taken into account, when using a measurement chain:

- Spatial and temporal resolution of the sensor: they represent the minimum sample space and the reacting time of the sensor;

- Accuracy: it represents how many digits can be acquired;

- Intrusivity of the sensor: the sensor must alter the quantity to be measured the least possible;

- Noise level on the output signal: the system must be as shielded as possible to external sources of noise;

- Stable data transmissions: the data have to be stored from a volatile memory(RAM) into a stable one. This data transmission must be as stable as possible, therefore short cables are preferred to long ones in order to reduce the possibility of signal's distortion.

Chapter 5

Experimental results and discussion

Once the setup has been successfully implemented, several experiments have been performed. These experiments aimed at verifying the effective control over all the parameters of interest: pulsation frequency, duty cycle and exit velocity.
All these parameters have been analysed by acquiring the output velocity at the exit of the slotted jet, by the use of a hot-wire anemometer, as shown in Figure 5.1. The signals have been subsequently post-processed with ad hoc Matlab algorithms.

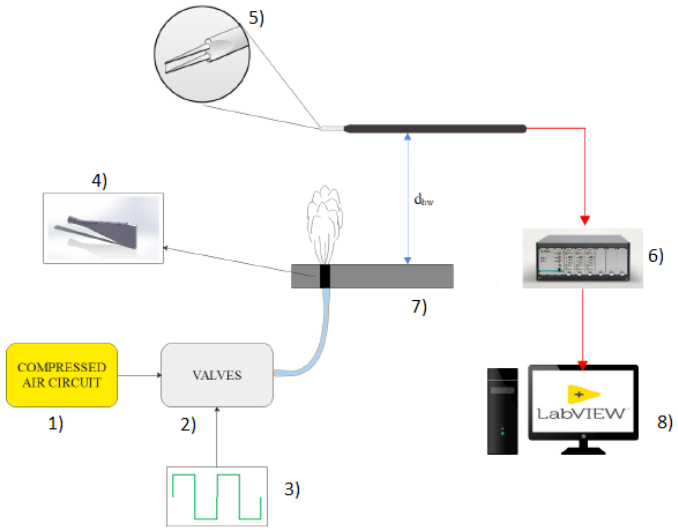

Figure 5.1: Schematic of the acquisition process: 1) Compressor; 2) Solenoidal valve; 3) Square wave generator; 4) Slotted jet; 5) Hot-wire; 6)DAQ; 7) 3-D printed pothole; 8) PC with NI-LabVIEW. Courtesy of A. Gessi.

Table 5.1 specifies all the experimental parameters.

Table 5.1: Summarizing table of the input parameters.

Input parameters	
Inlet pressure	3 bar
Sampling time	100 seconds
Pulsation frequency	From 50 Hz to 300 Hz (with steps of 50 Hz)
Duty cycle	25% , 50%, 75%
Orientation of the jet	Transversal to the crossflow
Shape of the slotted jet	Rectangular with guide vanes inside

For the analysis of only the pulsation frequency and the duty cycle, the signals were sampled at two different locations: at the exit of the solenoidal valve, and at the exit of the slotted jet, as shown in Figure 5.2 .

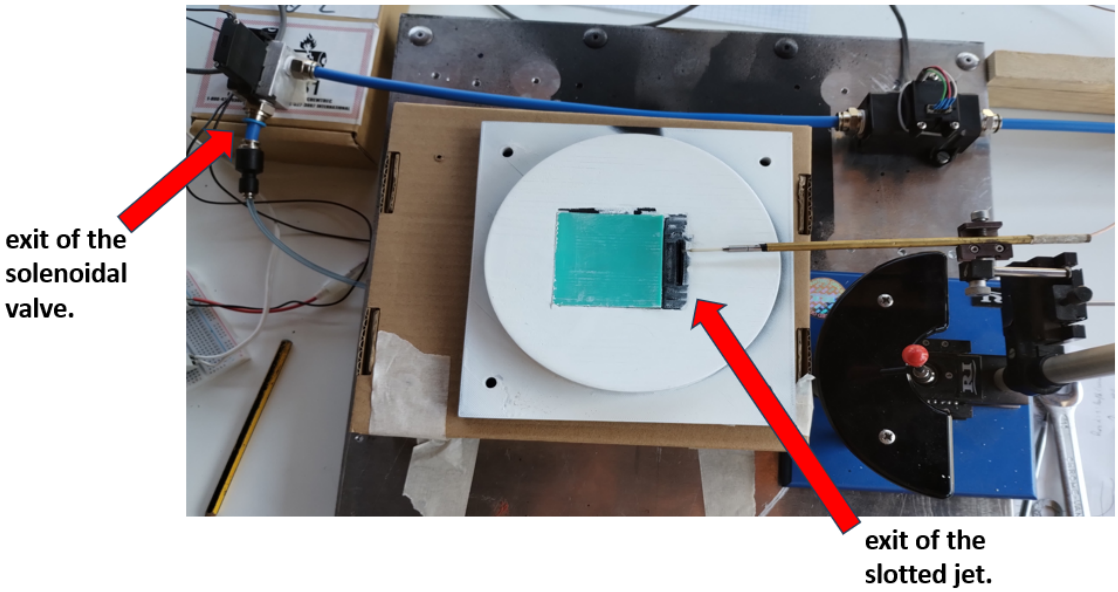

Figure 5.2: The two different sampling locations.

This is done because, due to the very narrow dimensions of the slotted jet, a bad positioning of the hot-wire probe with respect to the jet can bring to undesired effects which may affect the frequency and duty cycle estimations. As a matter of fact, the exit of the solenoidal valve has a much larger dimensions which facilitates the positioning of the probe.

5.1 Input/Output frequency analysis

For the frequency analysis it has been acquired the velocity at the exit of both the sampling locations, for all the different input values of pulsation frequency and duty cycle. Then, by using an ad hoc post-processing Matlab script, the Power Spectral Density of the signal has been derived.
The power spectral density (PSD) is the measure of the signal's power content versus frequency, and exploits the Fast Fourier Transform (FFT) mathematical tool. The Fourier transform is an extension of the Fourier series, which approaches a signal as a sum of sines and cosines, and it is used in order to project both continuous and

discrete data into the frequency domain.
Therefore any signal can be separated, or analysed, into a spectrum of discrete frequencies: indeed, the FFT algorithm takes frames of equal length and applies the DTFT (Discrete-Time Fourier Transform) to each frame. Then, it calculates the squared magnitude for each frequency bin and finds the average: the mean-square value is the "power" of the quantity, i.e. a measure of signal strength. Finally, the algorithm divides the mean-square value by the bandwidth to normalize it to a single hertz.
The result of the FFT is shown in Figure 5.3:

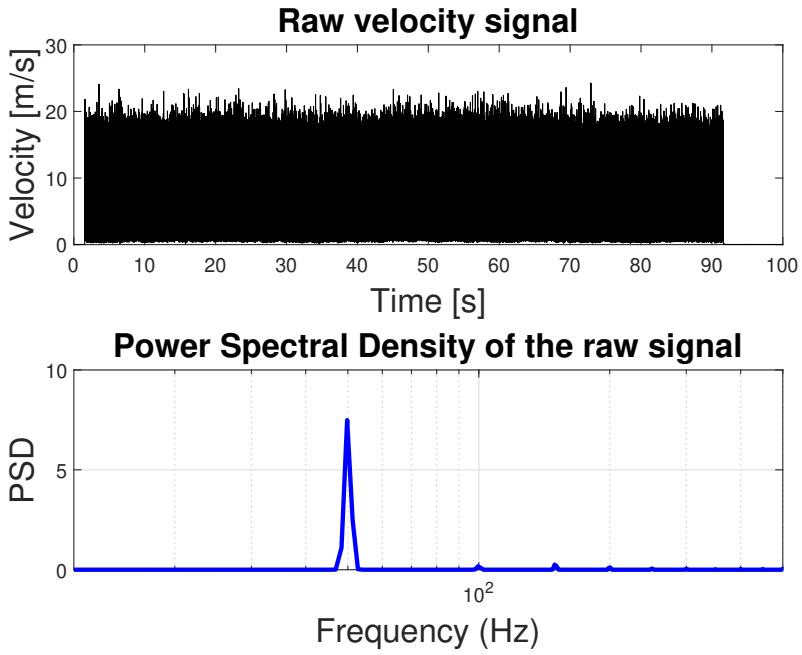

Figure 5.3: Power Spectral Density of a velocity signal.

Once obtained the Power Spectral Density of the signal, the output frequency is chosen as the one corresponding to the peak in the PSD of the signal itself.

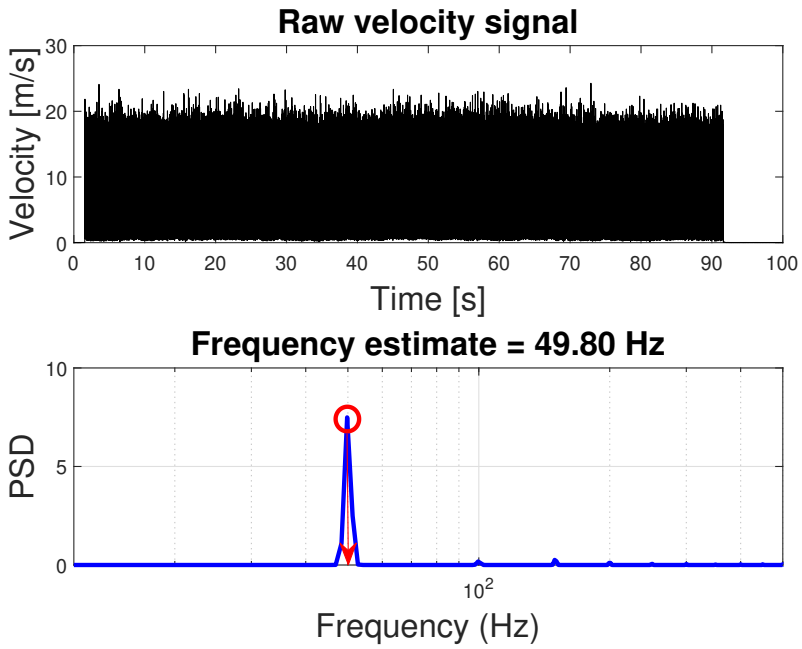

Figure 5.4: Frequency identification.

This procedure is repeated for all the input pulsation frequencies mentioned in Table 5.1, and the overall results are shown in Figure 5.5, Figure 5.6 and Figure 5.7.

In the following plots, the blue marks represent the values obtained at the exit of the slotted jet, while the black circles represent the values at the exit of the solenoidal valve. Moreover, voltage signals are identified with the the symbol V (which stands for voltage). For example V_{in} indicates the input voltage, that is the one coming from the DAQ, while V_{out} is the voltage measured by the hot-wire. On the other hand, U_{out} represents velocity signals.

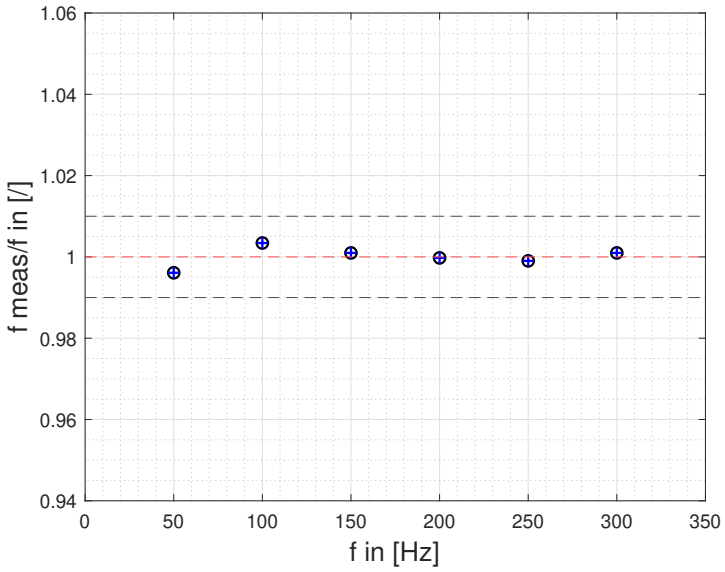

Figure 5.5: Frequency characterization for input duty cycles= 75%, for both the slotted jet(blue pluses) and the solenoidal valve(black circles).

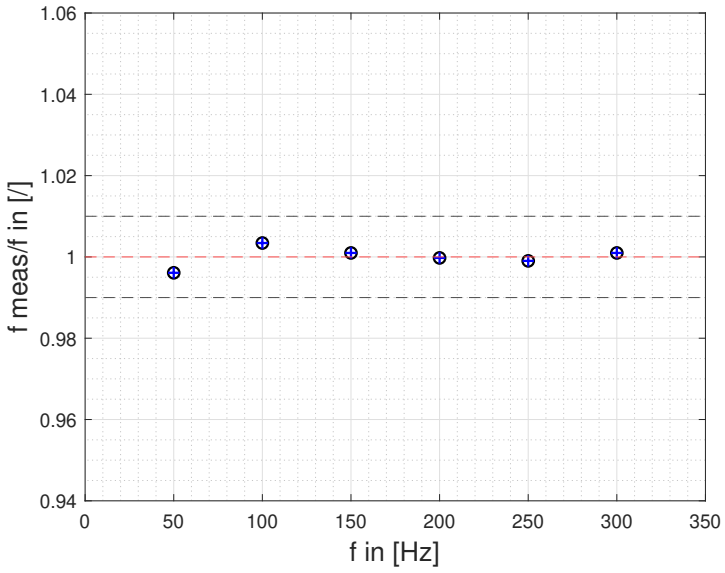

Figure 5.6: Frequency characterization for input duty cycles= 50%, for both the slotted jet(blue pluses) and the solenoidal valve(black circles).

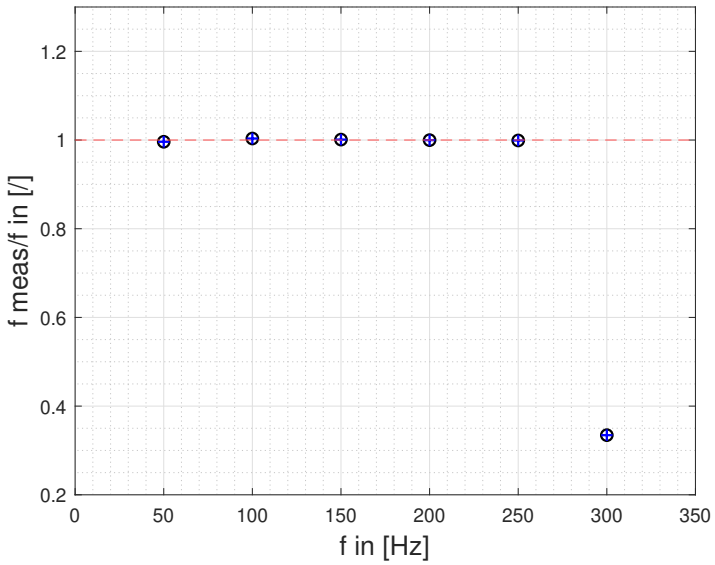

Figure 5.7: Frequency characterization for input duty cycle= 25%, for both the slotted jet(blue pluses) and the solenoidal valve(black circles).

As it can be seen, there is a very good agreement between the input pulsation frequency and the one obtained with the analysis of the velocity signal at the exit of the slotted jet, apart from the presence of a single outlier.
This outlier appears both at the exit of the slotted jet and at the exit of the solenoidal valve, for an input duty cycle of 25% and pulsation frequency of 300 Hz. Therefore, the cause behind the outlier has to be found elsewhere, that is in the analysis of the spectra of the signals, in particular for duty cycle = 25%.
However, an analysis of each single wave confirms this strange behaviour, which is remarked in Figure 5.8: indeed, it is possible to see only one peak in the voltage signal every three input peaks. This motivates the measured pulsation frequency to be one third of the input one.

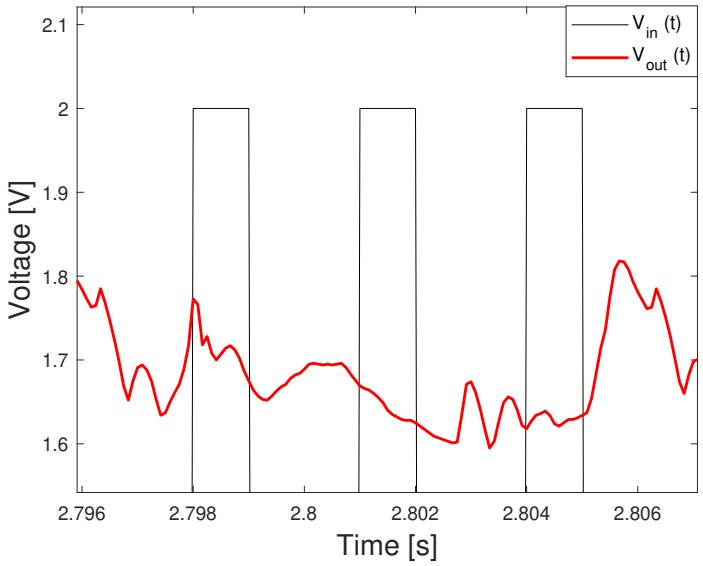

Figure 5.8: Raw voltage signals (black= DAQ input signal, red=hot-wire signal) for input pulsation frequency= 300 Hz and duty cycle= 25%; .

5.2 Analysis of the duty cycle

5.2.1 Phase average operation

For the analysis of the duty cycle at the output of the slotted jet, another mathematical tool is necessary: the phase average. Basically, it consists in the identification of each single wave inside the raw velocity signal, and then an average operation is performed.

This operation is needed because due to noise and other external disturbances, each velocity wave can be significantly different from the other ones, and this complicates the analysis of the output duty cycle. For the identification of each velocity wave, a different and "more reliable" wave must be taken as reference: hence, the square wave coming from the DAQ has been chosen.

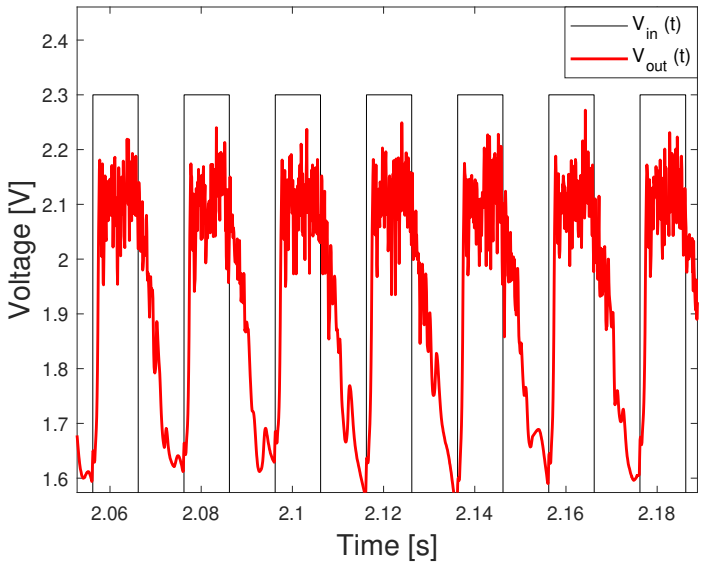

Figure 5.9: Raw voltage signals (black= DAQ input signal, red=hot-wire signal) for input pulsation frequency= 50 Hz and duty cycle= 50% .

The phase averaging procedure composes as follows:

- Identification of the indices corresponding to the high and low part of the reference signal: since the voltage signal coming from the DAQ is very stable, this operation is very accurate.

- Identification of every single velocity wave: each velocity wave is isolated according to the indices that have been previously found.

- Averaging of all the waves that have been identified.

This procedure gives as output a phase-averaged wave, shown in Figure 5.10:

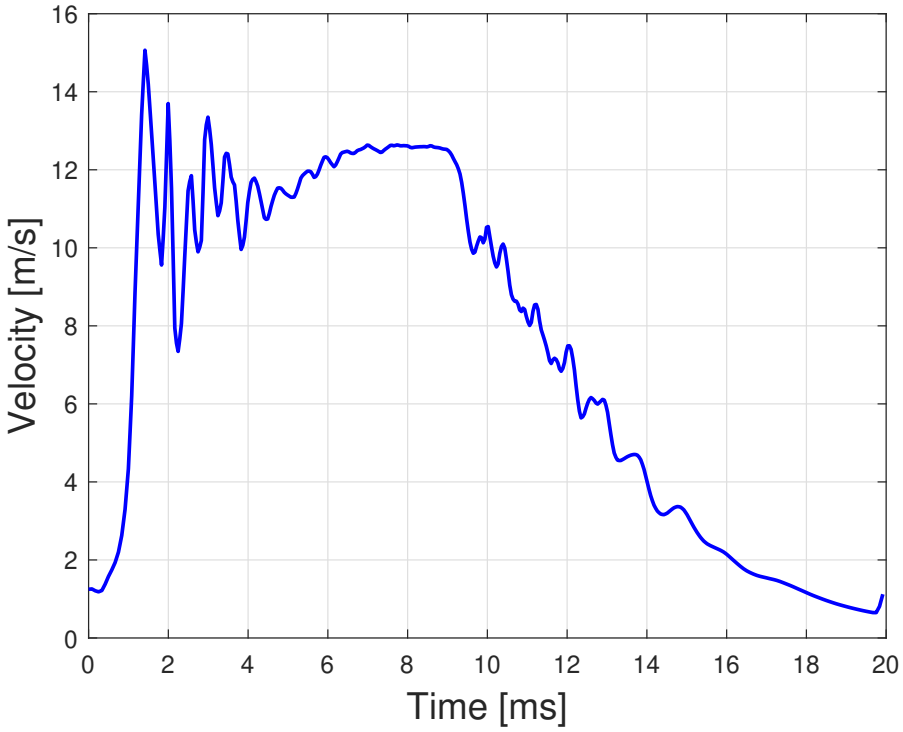

Figure 5.10: Velocity phase averaged signal with input pulsation frequency of 50 Hz and DC=50%.

From this kind of signal, several features can be noticed:

1. An opening delay time: each physical system is characterized by some delays in the response. Since the solenoidal valve does not open instantaneously, it will pass a certain amount of time between the opening signal and the effective opening of the valve. This delay is certified to be of the order of 1.25 milliseconds, for an input pressure of 2.5 bar.

2. A closing delay time: is the same behaviour as the previous one, but in this case it happens in the closing phase. This valve is certified with a closing delay time of 0.4 milliseconds, for an input pressure of 2.5 bar.

3. There is an overshoot in the opening phase: in the high part of the input signal,

the velocity does not settle down to a constant value instantaneously, but it takes a certain amount of time, an possesses a certain oscillatory dynamic.

4. The length of the duct downstream the valve influences the dynamic in the closing phase: as a matter of fact, when the signal is low, there is still some air trapped in the duct downstream the solenoidal valve, which is "seen" by the hot-wire even though it is the period in which the circuit is supposed to be closed. This explains why the closing phase measured by the hot-wire is much slower than the opening phase.

The effect described in 4) it is shown in Figure 5.11:

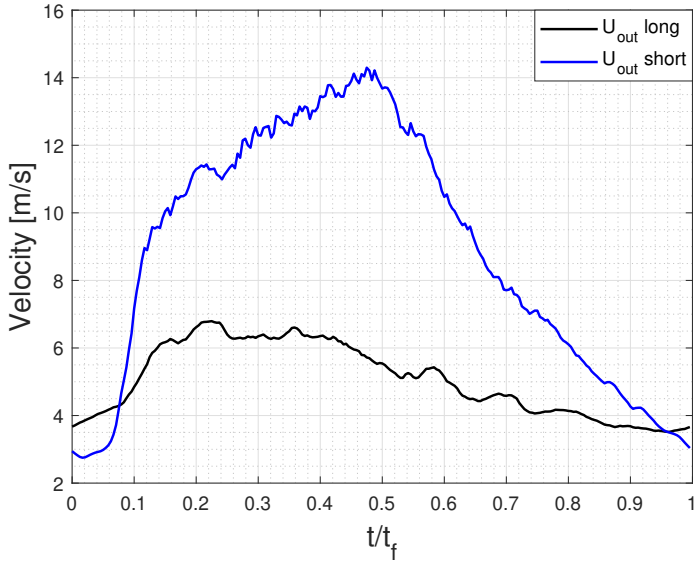

Figure 5.11: Different velocity phase averaged signals for long downstream duct(black) and short downstream duct(blue) for a frequency of 50 Hz and DC=50%.

5.2.2 Valve-delay estimation

Another important remark has to be made: as the pulsation frequency increases, the time period decreases significantly (from 20 ms for 50 Hz, up to 3.3 ms for 300

Hz). Considering the effect of duty cycle, the length of the period decreases even more. This is shown in the following label:

Table 5.2: Opening time based on input frequency and duty cycle.

Input parameters	DC=25%	DC=50%	DC=75%
Pulsation frequency = 50 Hz	5 ms	10 ms	15 ms
Pulsation frequency = 100 Hz	2.5 ms	5 ms	7.5 ms
Pulsation frequency = 150 Hz	1.67 ms	3.33 ms	5 ms
Pulsation frequency = 200 Hz	1.25 ms	2.5 ms	3.75 ms
Pulsation frequency = 250 Hz	1 ms	2 ms	3 ms
Pulsation frequency = 300 Hz	0.82 ms	1.65 ms	2.48 ms

Of course the shorter are period lengths, the more the above considerations will influence the outcoming signal at the exit of the jet. This means that the higher the pulsation frequency, the more the phase averaged signal will loose its similarity with a square wave. It can be noticed in Figure 5.12:

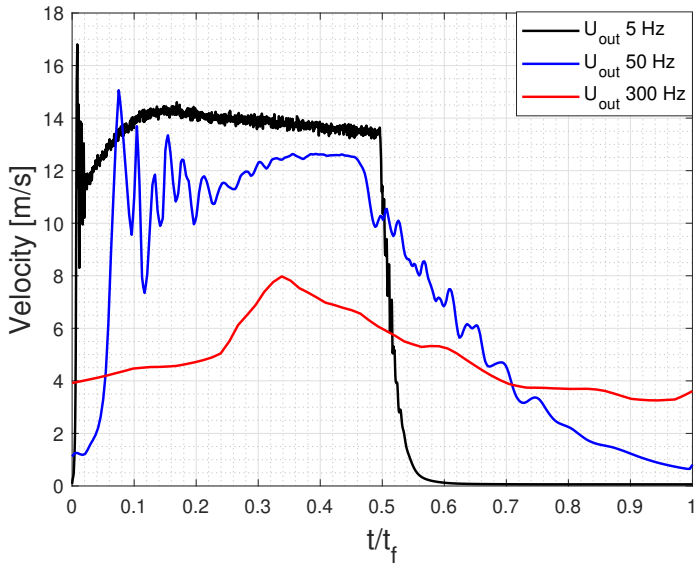

Figure 5.12: Different velocity phase averaged signals for long downstream duct(black) and short downstream duct(blue) for a frequency of 50 Hz and DC=50%.

The solenoidal valve used in this experiment is certified with an opening delay time of 1.25 milliseconds. But the delay time is defined as the time in which the velocity gets half its nominal value.
Indeed, an analysis of the real delay in the opening phase has been performed, showing an average delay time in the opening phase equal to 2.75 milliseconds:

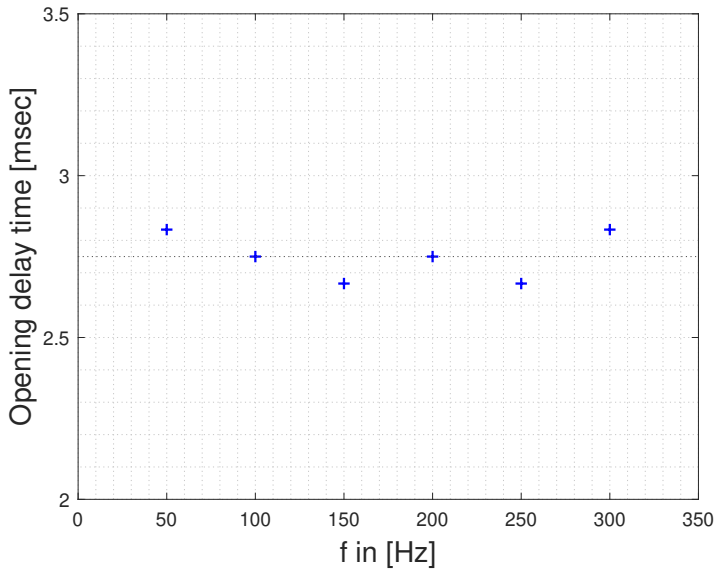

Figure 5.13: The delay times for different pulsation frequencies and DC=50%.

For low values of pulsation frequency, this delay does not affect the dynamic of the valve significantly and therefore the phase average signal presents a very good shape.
But as the pulsation frequency increases, this delay becomes more and more relevant on the valve's dynamics. Especially for 300 Hz of pulsation frequency and 25 % of duty cycle, the delay time is larger than the time in which the valve must remain opened. Therefore, the valve does not completely open itself, that it is already time to close.

All these considerations bring to the conclusion that the resulting value of the duty cycle is inevitably affected by these errors. They alter the phase averaged signal, which becomes more and more different from an ideal square wave signal.

5.2.3 Input/Output duty cycle analysis

The duty cycle is defined as the percentage of the ratio of pulse duration to the total period of the waveform. In this thesis, for the duty cycle estimation, an integral approach has been used, according to the Formula 5.1:

$$DC = \frac{\int_0^T u\,(t)\,dt}{U_{max} * T} \tag{5.1}$$

The formula expresses the duty cycle as a ratio between the area below the phase averaged signal and the area below a square wave signal with amplitude equal to U_{max} and period T. As it can be seen, the value of U_{max} is quite different from the mean value of the "high" part, and this brings to a DC underestimation.
On the other hand the closing phase is not instantaneous, making the integral area to be larger than it should and leading to a DC overestimation. Therefore, it is not possible assessing which one of these effects is dominant a priori, especially at high pulsation frequencies.
Moreover, the shape of the phase average signals is the main parameter that affects the values found for the duty cycle: as already pointed out, this effect is more evident at high pulsation frequencies.
After all these considerations, the duty cycle values for different pulsation frequencies are reported in the following Figures:

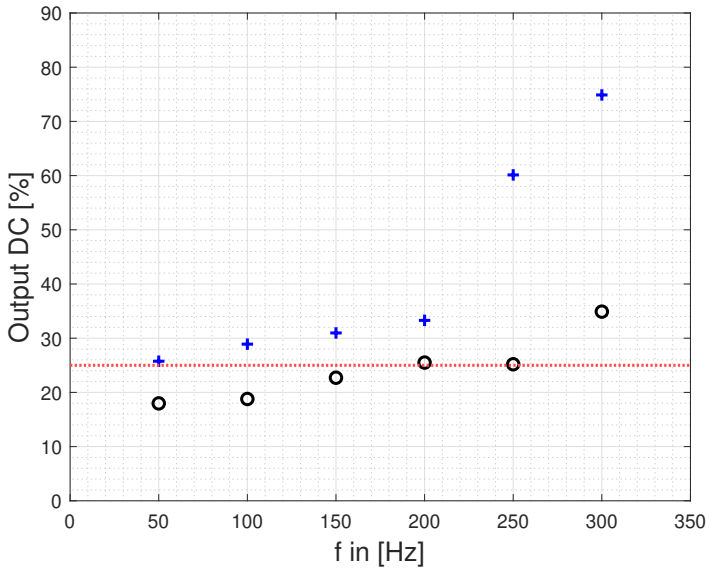

Figure 5.14: Duty cycle values for different input frequencies, both at the solenoidal valve(black circles) and at the jet(blue pluses).

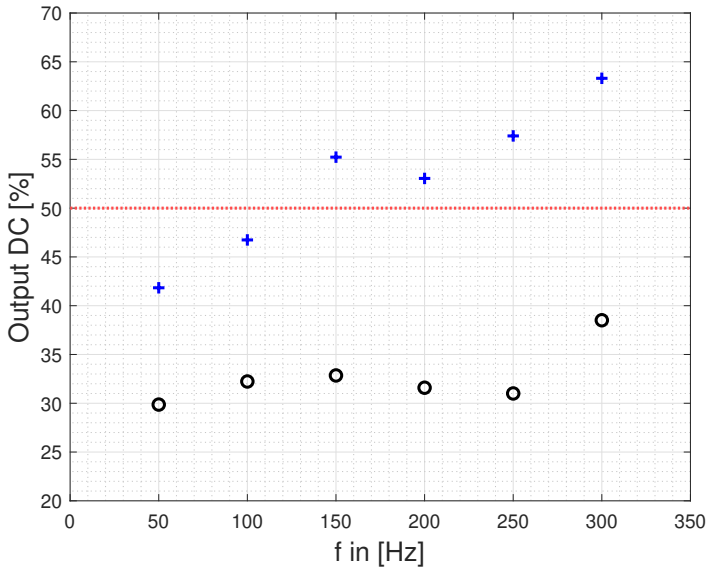

Figure 5.15: Duty cycle values for different input frequencies, both at the solenoidal valve(black circles and at the jet(blue pluses).

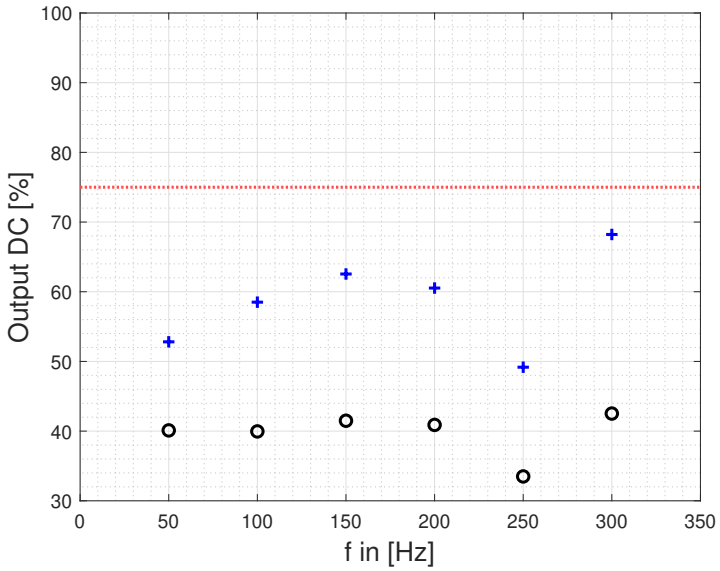

Figure 5.16: Duty cycle values for different input frequencies, both at the solenoidal valve(black circles) and at the jet(blue pluses).

It is evident that there is not a very good agreement between input and measured duty cycle, especially at high pulsation frequencies and for duty cycle=25%. This is explained by recalling that for DC=25%, the period during which the signal is in a high state, is very short and the above mentioned effects becomes even more relevant.

5.3 Control of jet-outlet velocity

All the velocity values obtained up to now are characterized by an upstream input pressure of 3 bar. Since the velocity ratio between the free-stream velocity and the jet's velocity is an important parameter which can alter the flow topology, by controlling the pressure it is possible to change this parameter.
In order to measure these values at the exit of the slotted jet, the setup has been positioned as it was in Figure 5.18 , and a continuous jet was generated. This was done for the same sampling locations of the previous experiment, but only for a

distance from the jet of 4 mm. Indeed, the velocity deficit with increasing distance from the jet is assumed to be the same as shown in Figures 5.20, 5.21, 5.22. The corresponding results are shown in Figure 5.17:

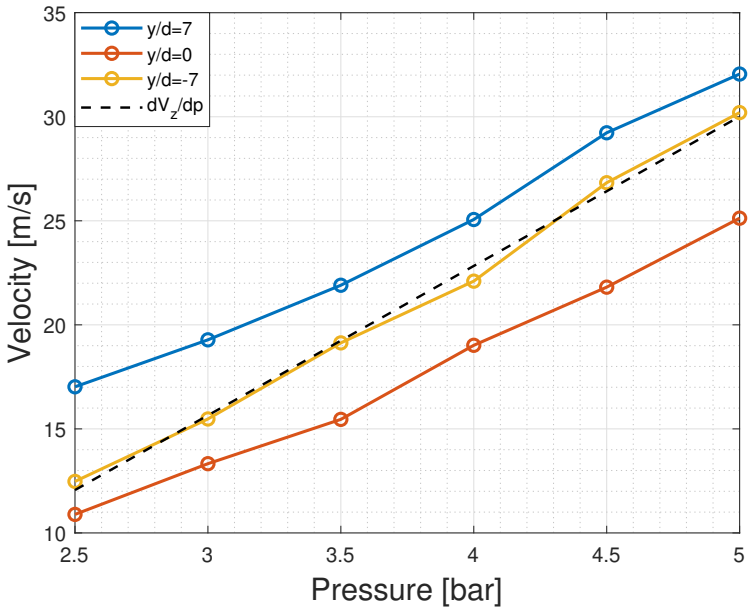

Figure 5.17: Spanwise characterization of the slotted jet with increasing input pressure.

The same spanwise velocity trend is observed, but a consistent increase in the output velocity is observed in all the three sampling locations. The black dashed line indicates the average trend of the output velocity in the streamwise direction (V_z) with increasing inlet pressure. As a matter of fact, by increasing the inlet pressure of 1 bar on average the output velocity increases of about 6.3 m/s.

5.4 Transverse velocity profiles

For a complete characterization of the jet, the spanwise velocity profiles were acquired. The experimental setup and the corresponding frame of reference are shown in Figure 5.18, whereas its scheme is presented in Figure 5.19:

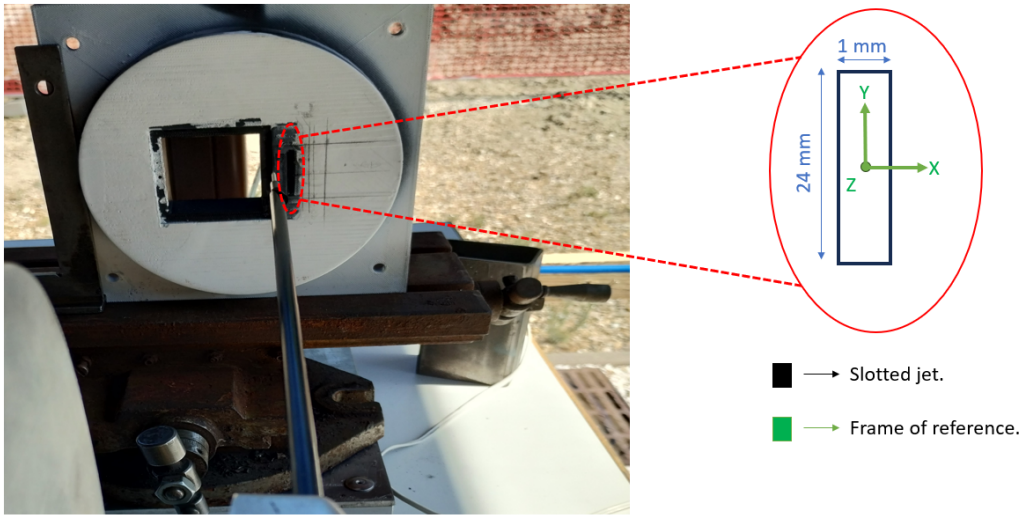

Figure 5.18: Initial setup disposition for the spanwise velocity profiles acquisition.

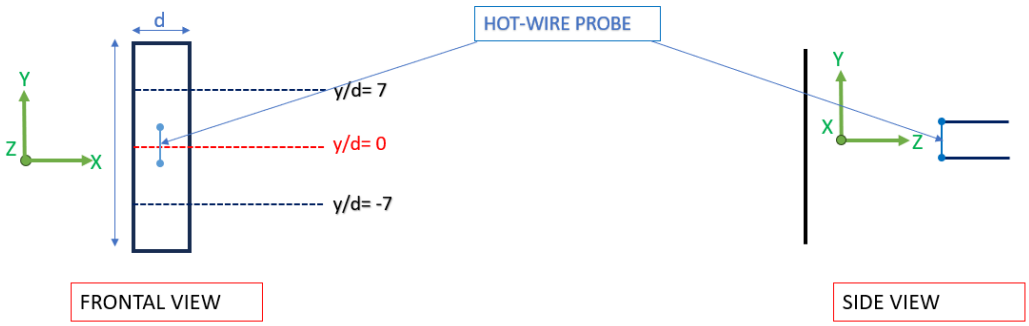

Figure 5.19: Scheme of the initial setup disposition for the spanwise velocity profiles acquisition.

The frame of reference is chosen as follows:

- Along X axis: chordwise direction;
- Along Y axis: spanwise direction;
- Along Z axis: streamwise direction;
- d= 1 mm.

The velocity profiles have been obtained by keeping the hot-wire probe parallel to the spanwise direction. The movement in the chordwise direction was regulated by a stepper motor, whereas the movement along the streamwise direction was performed by using a 2-axis cross slide bench. Finally, the spanwise location has been set by using some shimming objects with predetermined thicknesses. The acquisition procedure is here briefly summarized:

- 3 spanwise sampling locations: centerline (y/d=0), y/d= 7 and y/d= -7;
- 3 streamwise sampling locations: z/d= 4, z/d= 8, z/d= 16;
- 67 chordwise samples according to a predetermined spatial grid, considering a spreading angle of 12°;
- The slotted jet is aligned with the z axis.

5.4.1 Velocity decay

The velocity decay in the streamwise direction can be appreciated in the following plots:

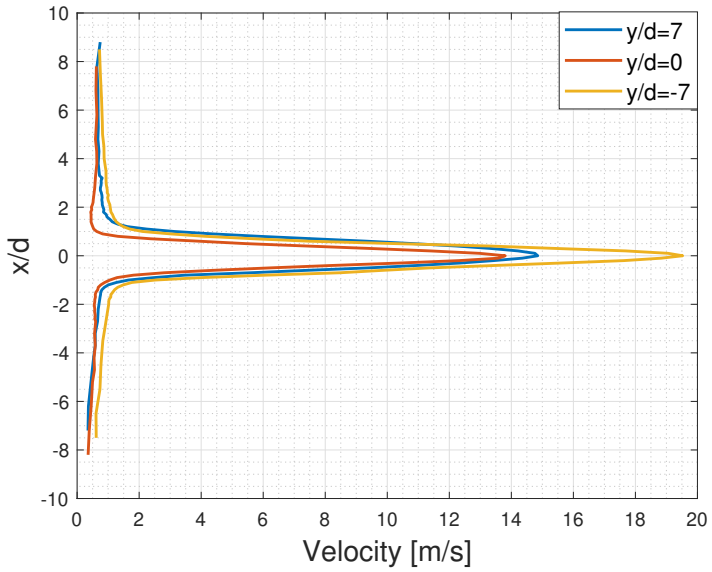

Figure 5.20: Chordwise velocity profile for different spanwise locations, at z/d=4.

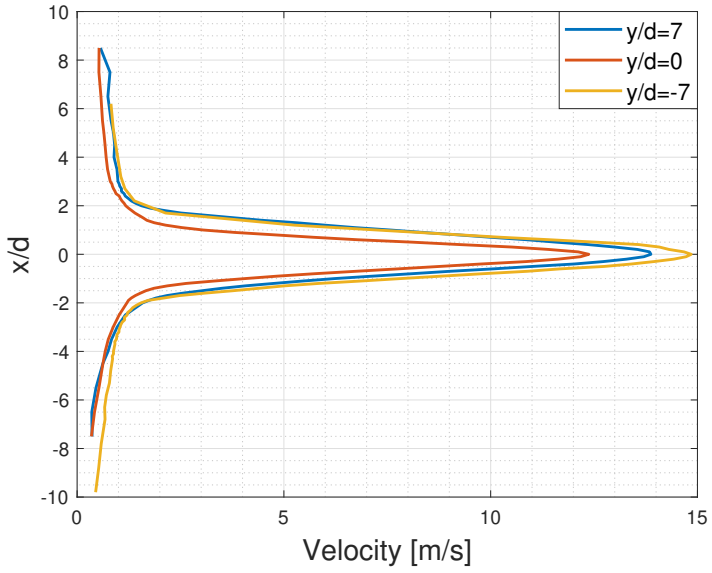

Figure 5.21: Chordwise velocity profile for different spanwise locations, at z/d=8.

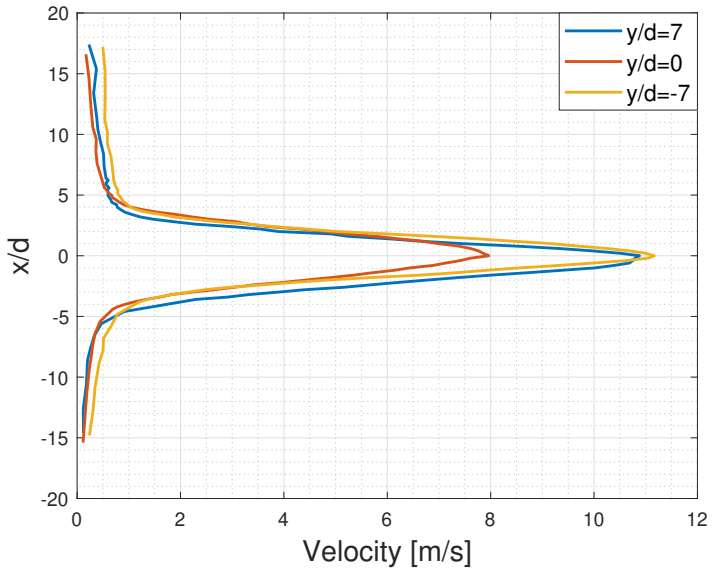

Figure 5.22: Chordwise velocity profile for different spanwise locations, at z/d=16.

As expected, as the distance from the slotted increases the velocity reduces. But these plots show that there is an unexpected spanwise behaviour: as a matter of fact, the velocity at the exit of the slotted jet is not uniform at all, moving along the y coordinate. In particular, the velocity at the two ends significantly differ, and the central part of the jet is the slowest position. This non-uniformity requires a deeper analysis and a different setup positioning.

5.5 Spanwise velocity profiles

For the new experimental acquisitions, the setup disposition is shown in Figure 5.23:

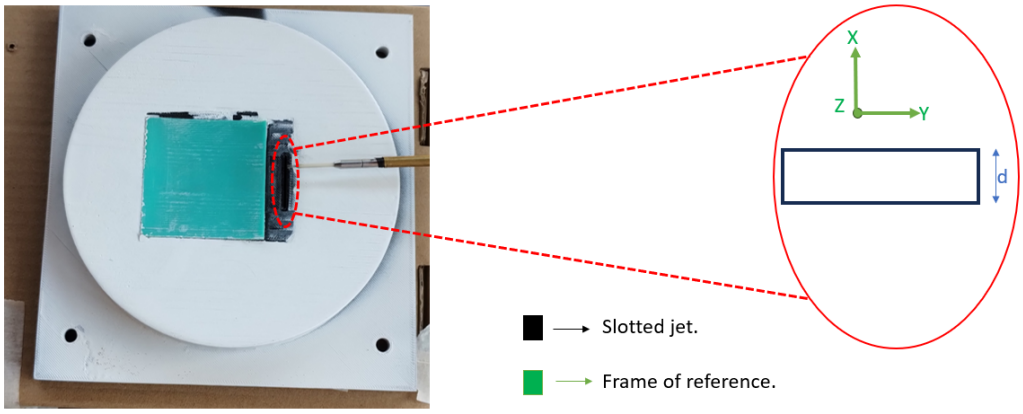

Figure 5.23: Different setup disposition for the spanwise velocity profiles acquisition.

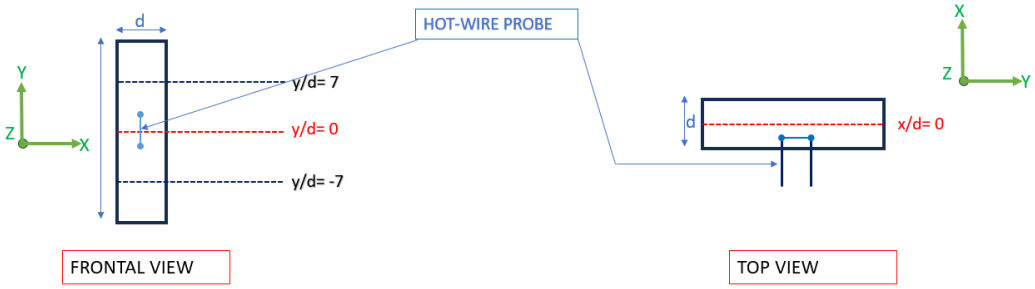

Figure 5.24: Different setup disposition for the spanwise velocity profiles acquisition.

As before, the velocity profiles have been obtained by keeping the hot-wire probe parallel to the spanwise direction, but there are some differences:

- 5 chordwise sampling locations: centerline (x/d=0), x/d= ±0.5 and x/d= ±1;

- 110 spanwise samples according to a pre-optimised spatial grid, considering a spreading angle of 12°;

Results are shown in Figure5.25:

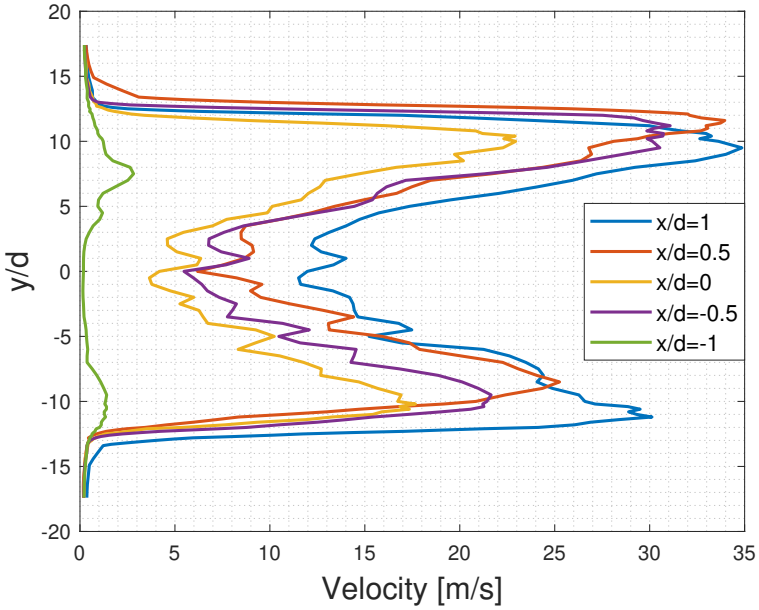

Figure 5.25: Spanwise characterization of the slotted jet.

These data are in accordance with the ones found in the previous experiment, but highlight a very non-uniform spanwise behaviour of the jet. This may be caused by the guide vanes inside the slotted jet, which may not work appropriately. A new jet design seems to be the best solution possible, and it will discussed in the "Future works" section.

Chapter 6

Conclusions and future works

6.1 Conclusions

The objective of the present thesis is the development and characterization of an active jet for convective-heat transfer enhancement. In particular, the device comprises an electric circuit driving a solenoidal valve and a diffuser creating the planar jet. The diffuser is embedded in a plug for the installation in the Long Pipe facility in CICLoPE laboratory.

The electronic circuit has been built and the outgoing signal has been successfully generated: a square wave signal controlled in frequency, duty cycle and output velocity has been obtained. Then, by using a hot-wire anemometer, the velocity at the exit of the slotted jet has been analyzed in order to check the correspondence with the input parameters.

From this signal, we carefully checked that the pulsation frequency corresponded to the one set as input from Lab-VIEW: this has been done with the use of the Power Spectral Density of the signal. A very good correspondence between the input and output values is found, except for a single outlier for a pulsation frequency of 300 Hz and DC 25%. This deviation may derive either from a non-optimal positioning of the hot-wire probe or may be caused by the geometry of the slotted jet. A more detailed analysis of the spectra of the signal will clarify this doubt.

Concerning the duty cycle, things were slightly more complicated: since it is not so easy to have a clear distinction between the "high" state and the "low" state of the signal, the value of the duty cycle is not very precise. Therefore, there is an very large difference between the input value and the one obtained at the output.
Moreover, it also appeared that the output signal at the jet's exit never goes back to zero, even in the "off" state, and that this behaviour is more and more evident the higher we go with the pulsation frequency. These anomalous behaviours are supposed to happen because the air inside the duct in between the solenoidal valve and the jet diffuser keeps flowing outside for a short while even when the circuit should be closed. As a matter of fact, by comparing two signals with the same input parameters but different pipe lengths, it is visible that the shorter duct resembles much more closely the input signal, that is a square wave.
Successively, an analysis about the variation of the velocity at the exit of the solenoidal valve has been carried out, for different pressure values. The results show an increase in the output velocity of approximately 6.3 m/s for every 1 bar increase in the inlet pressure.
Finally, I have done a spanwise characterization of the diffuser. Once again, it is revealed an unexpected behaviour, with a non-symmetric velocity profile at the two ends and a much lower speed at the center of the jet. A parametric study confirms that the jet is supposed to operate inside a region of appreciable stall, and the guide vanes inside of it may not be sufficient in order to prevent the stall. Therefore, a new design seems to be required.

6.2 Future works

6.2.1 Jet optimization

Since the results shown in Chapter 5 highlight an unexpected spanwise behaviour of the jet, this may be in accordance with a regime of transitory stall. A possible solution could be the design of a different geometry for the jet.
For the new jet's design, the reference equation is 6.1, in which the constrained parameters are W1=3.96 mm and L=12 mm (half of the jet's length).

$$\frac{W1}{2} + N * tg\,(\theta) = L \tag{6.1}$$

A plot with all the combinations of N/W1 and θparameters that fulfill equation 6.1 is shown in Figure 6.1:

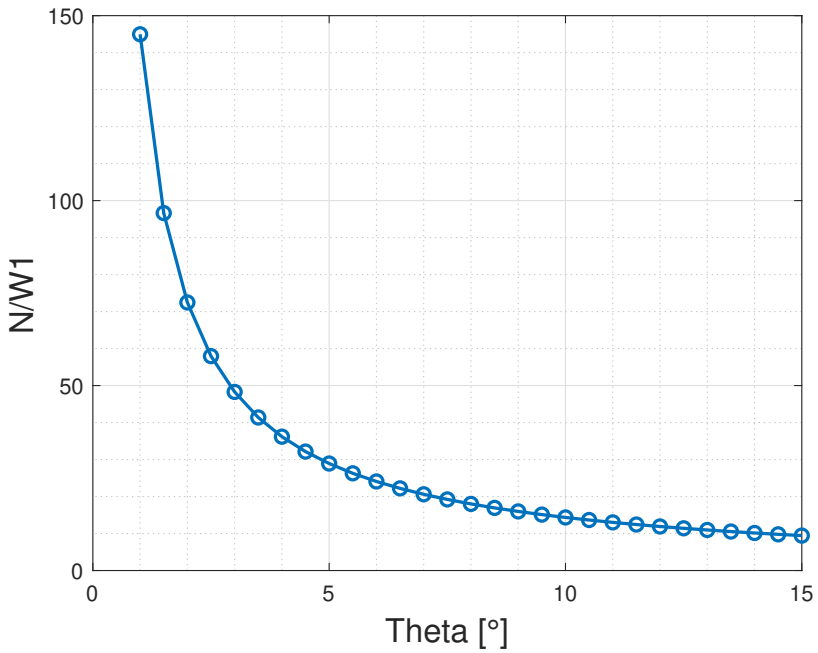

Figure 6.1: N/W1 values for different θ angles.

A reasonable value for N can be 163.8 mm, which can be obtained with a θangle

of 3.5 °: this would imply a N/W1 value of 41.4, resulting in the green point in Figure 4.4.

For every available value of theta and N/W1, the diffuser always falls inside the region of large appreciable stall. One possible solution is to increase the value of W1, which would mean increasing the diameter of the rounded part of the jet. This solution has to be carefully designed, because it may affect also the diameter of the pipe which connects the solenoidal valve to the slotted jet.

6.2.2 Background Oriented Schlieren

A very interesting and non-intrusive method is represented by the imaging technique known as Background Oriented Schlieren (BOS) . In particular, BOS is an optical density visualization technique, belonging to the same family as Schlieren photography, shadowgraphy or interferometry.
In contrast to these older techniques, BOS uses correlation techniques on a background dot pattern to quantitatively characterize compressible and thermal flows with good spatial and temporal resolution. As a matter of fact, due to refractive phenomena arising from air density changings, the dots of a background grid appear to be shifted. By evaluating these shifts, it is possible to quantify the field of motion of the particles.
The main advantages of this technique are the experimental simplicity and the robustness of correlation-based digital analysis.[43] This interesting approach would also eliminate the problems related to the small dimensions of the slotted jet and the bad-positioning of the hot-wire probe.

6.2.3 Wind tunnel implementation

The 3-D printed pothole must be inserted inside the wind tunnel, after the mounting of the PCB. Successively we operate the wind tunnel, the slotted jet and the PCB. The effectiveness of the control parameters about the heat transfer enhancement are evaluated with the use of an Infrared thermal-imaging camera. The acquisition process is supposed to be the same adopted by Castellanos et al. [4]

Bibliography

[1] https://www.mcgill.ca/mecheng/undergrad/curriculum/mechlab/heat.

[2] J.S. Slongo, J. Gund, T.A.R. Passarin, D.R. Pipa, J.E. Ramos, L.V. Arruda, F.N. Junior, Effects of Thermal Gradients in High-Temperature Ultrasonic Non-Destructive Tests. Sensors 2022, 22, 2799. https://doi.org/10.3390/s22072799

[3] Z. Zhang, X. Ren, Causal relationships between energy consumption and economic growth, Energy Proc., 5 (2011), pp. 2065-207 .

[4] R. Castellanos, G. Salih, M. Raiola, A. Ianiro, S. Discetti, (2023), Heat transfer enhancement in turbulent boundary layers with a pulsed slot jet in crossflow, Applied Thermal Engineering, vol. 219, part C.

[5] G. Buresti, Elements of fluid dynamics, Imperial College Press (Vol 3), 2012. DOI: 10.13140/RG.2.2.31647.46249/13.

[6] https://upload.wikimedia.org/wikipedia/commons/9/9d/Jet_engine-kn.svg

[7] https://commons.wikimedia.org/wiki/File:RAKON_STP2734B_LF_OCXO_temperature-control_circuitry.jpg

[8] https://www.britannica.com/science/thermodynamics

[9] https://www.albert.io/blog/difference-between-temperature-and-heat/

[10] J.Horacek, Measurement of edge electrostatic turbulence in the TCV tokamak plasma boundary, PhD Thesis No 3524,Ecole Polytechnique Federale de Lausanne (EPFL), Lausanne, Switzerland.

[11] H. Tennekes and J. L. Lumley, A First Course in Turbulence, MIT Press, 1972.

[12] https://www.cfdsupport.com

[13] https://www.thermopedia.com/de/content/1092/

[14] http://www.lcad.icmc.usp.br

[15] J. H. Hussein, S. P. Capp, and W. K. George. Velocity measurements in a high reynolds number, momentum conserving, axisymmetric, turbulent jet. J. Fluid. Mech, (1994).

[16] J.J. Kuang, X.L. Wang, T.J. Lu, T. Kim, Role of Laminar Length of Round Jet Impinging on Metal Foams (2015). Journal of Thermophysics and Heat Transfer. 30. 1-8. 10.2514/1.T4567.

[17] J. H. W. Lee , V. H. Chu, Turbulent Jets and Plumes: a Lagrangian Approach, Springer New York, NY, (2003).

[18] B. Khanal, K. Knowles, A. Saddington, Computational Investigation of Cavity Flow Control Using a Passive Device (2012). Aeronautical Journal -New Series-. 116. 153-174.

[19] A.M. Jacobi, R.K. Shah, Heat transfer surface enhancement through the use of longitudinal vortices: A review of recent progress, Exp. Therm Fluid Sci. 11 (3) (1995) 295-309, Generation and Structure of Vortical Flows for Heat Transfer Enhancement.

[20] K. Kataoka, M. Suguro, H. Degawa, K. Maruo, I. Mihata, The effect of surface renewal due to largescale eddies on jet impingement heat transfer, Int. J. Heat Mass Transfer 30 (3) (1987) 559-567.

[21] T. Liu, J. Sullivan, Heat transfer and flow structures in an excited circular impinging jet, Int. J. Heat Mass Transfer 39 (17) (1996) 3695-3706.

[22] E. Mladin, D. Zumbrunnen, Local convective heat transfer to submerged pulsating jets, Int. J. Heat Mass Transfer 40 (14) (1997) 3305-3321.

[23] Margason RJ. 1993. Fifty years of jet in cross flow research. Comput. Exp. Assess. Jets Cross Flow, AGARD-CP 534, Advis.Group Aeronaut. Res. Dev., Washington, DC.

[24] H. Johari, M. Pacheco-Tougas, J. Hermanson, Penetration and mixing of fully modulated turbulent jets in crossflow, AIAA J. 37 (7) (1999) 842-850.

[25] A. Eroglu, R.E. Breidenthal, Structure, penetration, and mixing of pulsed jets in crossflow, AIAA J. 39 (3) (2001) 417-423.

[26] T.F. Fric, A. Roshko, Vortical structure in the wake of a transverse jet, J. Fluid Mech. 279 (1994) 1-47.

[27] D.S. Liscinsky, B. True, J. Holdeman, Crossflow mixing of noncircular jets, J. Propuls. Power 12 (2) (1996) 225-230.

[28] M.W. Plesniak, D.M. Cusano, Scalar mixing in a confined rectangular jet in crossflow, J. Fluid Mech. 524 (2005) 1-45.

[29] J.E. Broadwell, R.E. Breidenthal, Structure and mixing of a transverse jet in incompressible flow, J. Fluid Mech. 148 (1984) 405-412.

[30] J. Andreopoulos, W. Rodi, Experimental investigation of jets in a crossflow, J. Fluid Mech. 138 (1984) 93-127.

[31] S.H. Smith, M.G. Mungal, Mixing, structure and scaling of the jet in crossflow, J. Fluid Mech. 357 (1998) 83-122.

[32] Unibo (2022). CICLoPE wind tunnel.

[33] H.H. Bruun, Hot-wire anemometry - Principles and signal analysis, Oxford University Press, (1995).

[34] Rathakrishnan, E. (2007). Instrumentation, Measurements, and Experiments in Fluids,Second edition, CRC Press.

[35] G. Zambonini, Unsteady dynamics of corner separation in a linear compressor cascade, (2016).

[36] https://www.honeywell.com.

[37] https://www.mks.com.

[38] A. Torre, A. Ianiro, S. Discetti, G.M. Carlomagno, Evaluation of anisotropic tangential conduction in printed-circuit-board heated-thin-foil heat flux sensors, Int. J. Heat Mass Transfer 127 (2018) 1138-1146.

[39] https://www.smc.eu.

[40] https://www.ni.com.

[41] A.C. Avelar, S.Uyeno, A.G.Marto, O.A.de Faria Mello, C.F.Truyts, velocity profile and turbulence intensity measurements in the TA-2 wind tunnel,18th International Congress of Mechanical Engineering,November 6-11, 2005, Ouro Preto, MG.

[42] https://en.wikipedia.org/wiki/Data_acquisition.

[43] M.Raffel, Background-oriented schlieren (BOS) techniques, review article,Springerlink.com, Exp Fluids (2015) .